Numerical simulation of thermal stratification in Lake Qiandaohu using an improved WRF-Lake model

Wang, Xiwen; Wang, Weijia; He, Yuan; Zhang, Shulei; Huang, Wei; Woolway, R. Iestyn; Shi, Kun; Yang, Xiaofan

Journal of Hydrology

DOI:
10.1016/j.jhydrol.2023.129184

Published: 01/03/2023

Peer reviewed version

Numerical simulation of thermal stratification in Lake Qiandaohu using an improved WRF-Lake model

Xiwen Wang[a,b], Weijia Wang[b,c], Yuan He[d], Shulei Zhang[e], Wei Huang[a], R. Iestyn Woolway[f], Kun Shi[b,c*], Xiaofan Yang[d*]

[a] Key Laboratory of Western China's Environmental Systems (Ministry of Education), College of Earth and Environmental Sciences, Lanzhou University, Lanzhou, 730000, China

[b] Taihu Laboratory for Lake Ecosystem Research, State Key Laboratory of Lake Science and Environment, Nanjing Institute of Geography and Limnology, Chinese Academy of Sciences, Nanjing 210008, China

[c] University of Chinese Academy of Sciences, Beijing 100049, China

[d] State Key Laboratory of Earth Surface Processes and Resource Ecology, Faculty of Geographical Science, Beijing Normal University, Beijing 100875, China

[e] School of Atmospheric Sciences, Sun Yat-sen University, Guangzhou, China

[f] School of Ocean Sciences, Bangor University, Menai Bridge, Anglesey, Wales

Corresponding author:

Kun Shi: kshi@niglas.ac.cn

Xiaofan Yang: xfyang@bnu.edu.cn

Abstract

Lake thermal stratification is important for regulating lake environments and ecosystems and is sensitive to climate change and human activity. However, numerical simulation of coupled hydrodynamics and heat transfer processes in deep lakes using one-dimensional lake models remains challenging because of the insufficient representation of key parameters. In this study, Lake Qiandaohu, a deep and warm monomictic reservoir, was used as an example to investigate thermal stratification via an improved parameterization scheme of the Weather Research and Forecast (WRF)-Lake. A comparison with in situ observations demonstrated that the default WRF-Lake model was able to simulate well the seasonal variation of the lake thermal structure. However, the simulations exhibited cold biases in lake surface water temperature (LSWT) throughout the year while generating weaker stratification in summer, thereby leading to an earlier cooling period in autumn. With an improved parameterization (i.e., via determination of initial lake water temperature profiles, light extinction coefficients, eddy diffusion coefficients and surface roughness lengths), the modified WRF-Lake model was able to better simulate LSWT and thermal stratification. Critically, employing realistic initial conditions for lake water temperature is essential for producing realistic hypolimnetic water temperatures. The use of time-dependent light extinction coefficients resulted in a deep thermocline and warm LSWT. Enlarging eddy diffusivity led to stronger mixing in summer and further influenced autumn cooling. The parameterized surface roughness lengths mitigated

the excessive turbulent heat loss at the lake surface, improved the model performance in simulating LSWT, and generated a warm mixed layer. This study provides guidance on model parameterization for simulating the thermal structure of deep lakes and advances our understanding of the strength and revolution of lake thermal stratification under seasonal changes.

Keywords: Thermal stratification; Lake/reservoir; Numerical simulation; WRF-Lake; Parameter sensitivity

1. Introduction

Thermal stratification is an important physical process in many lakes/reservoirs that modulates their response to climate change and maintains lake ecosystem functions (Donis et al., 2021; Till et al., 2019). Stratification in lakes is mediated by the complex non-linear interactions between the lake surface and the atmosphere. It is influenced by atmospheric forcing and lake-specific properties, such as water transparency and geomorphological (depth, surface area) factors (Kraemer et al., 2015; Richardson et al., 2017). Although recent studies have reported a mixing regime shift in large lakes (Anderson et al., 2021), a fundamental and predictive understanding of lake stratification is still obscured due to the scarcity of in situ observations. Numerical simulations provide an opportunity to compensate for the space and time limitations of observations (Piccolroaz et al., 2020) and diagnose the effects of potential impact factors (Woolway et al., 2020; Woolway et al., 2019). Growing computational power further allows the coupling of lake and climate models to simulate lake–atmosphere interactions. However, the demand for computing efficiency in large-scale and long-term simulations restricts the application of sophisticated three-dimensional hydrodynamic models (Zamani et al., 2021). One-dimensional (1D) lake models, which simplify lake physical processes but require relatively minimal calibration, have been demonstrated to be effective tools for simulating thermal stratification at larger scales (Bruce et al., 2018; Stepanenko et al., 2010).

There are two types of one-dimensional lake models based on different numerical discretization methods: bulk (or integral) models and models based on the finite-difference scheme (Stepanenko et al., 2010). For example, the Freshwater Lake model (FLake) (Mironov, 2008), as a representative bulk lake model, has been incorporated into a set of climate models with high computational efficiency (Balsamo et al., 2012; Thiery et al., 2014b). Evaluations of the FLake model have shown that it is suitable for reproducing LSWT and thermal structure in shallow lakes but fails to simulate the development of thermal stratification in deep lakes as it does not directly solve the physical processes (Huang et al., 2019; Thiery et al., 2014a). The models based on the finite-difference scheme include eddy diffusion models and turbulent-kinetic (k-ε) models (Perroud et al., 2009). Eddy diffusion models use semi-empirical parameterization for the representation of turbulent fluxes. The k-ε models solve two equations including turbulent kinetic energy and its dissipation rate. Eddy diffusion models are inexpensive and proven to produce more accurate epilimnion temperature, whereas the k-ε models are more complicated but performed better for simulating thermocline depth (Guo et al., 2021). Eddy diffusion models are ideal candidates for coupling to climate/earth system models because of their relatively low cost and better representation of mixing processes compared to FLake. For example, the Hostetler lake model and its successors have been implemented in the community land surface model (CLM-Lake) (Oleson et al., 2013), common land model (CoLM-Lake) (Dai et al., 2018a), and the Weather Research and Forecast model (WRF-Lake)

(Gu et al., 2015). Previous studies have shown that the lake component of WRF-Lake outperformed FLake and other lake models based on turbulent closure schemes when simulating summer stratification in Lake Valkea-Kotinen, a small shallow lake in southern Finland (Stepanenko et al., 2014). It has also been suggested that WRF-Lake better describes the temporal variation of the total water column temperature than FLake and CoLM-Lake in Lake Nam Co, a large and deep lake on the Qinghai-Tibet Plateau (Huang et al., 2019). Hostetler model shows smaller biases compared to those utilizing more complicated algorithms when used for global application (Guo et al., 2021) and offers a marked degree of flexibility for specific lake applications (Martynov et al., 2010).

The WRF-Lake model has been utilized to simulate physical processes in a variety of lakes, from shallow to deep systems as well as those situated across warm and cold climatic regions (Gu et al., 2015; Gu et al., 2016; Huang et al., 2019; Su et al., 2022; Wu et al., 2020; Xiao et al., 2016; Xu et al., 2016). The performance of WRF-Lake is highly sensitive to key model parameters, notably the eddy diffusivity, light extinction coefficient, temperature of maximum water density for brackish water simulations, and surface roughness lengths of lake surface (Huang et al., 2019). These parameters are lake-specific and simplified in WRF-Lake. Such simplification may be sufficient for global-scale analysis, in which the uncertainties for specific lakes of a single model can either be filtered directly or compensated by ensemble simulations to reveal large-scale patterns. But for regional-scale simulations, the model

parameters related to lake characteristics have to be carefully tuned to achieve the required accuracy. Gu et al. (2015) suggested that although LSWT in relatively shallow lakes (e.g., Lake Erie) can be well captured, the vertical heat transfer process predicted by WRF-Lake is underestimated for deep lakes (e.g., Lake Superior) and leads to large biases in LSWT. Previous parameter sensitivity analyses demonstrated that the deficiency of WRF-Lake can be improved by enlarging the eddy diffusivity by a factor of 10^2–10^5, which has been proven to be effective in simulating the thermal structure of Lake Nam Co (Huang et al., 2019; Wu et al., 2020). However, another study at the Laurentian Great Lakes found that the parameterization scheme presented by Gu et al. (2015) only exerted a limited influence on Lake Michigan (~ 147.5 m at the mooring site) (Xiao et al., 2016). A recent study based on the offline version of WRF-Lake in the deep Reservoir Nuozhadu utilized a more elaborate calibration for eddy diffusivity, in which an enhanced term was added and enlarged for deep layers (Wang et al., 2019). Therefore, it is evident that the influence and uncertainty of eddy diffusivity on simulating thermal structures in deep lakes are quite diverse yet unclear, which requires proper calibration in different lakes.

Moreover, the light extinction coefficient can substantially alter the thermal structure of lakes by regulating the vertical heat transfer process (Read and Rose, 2013; Rose et al., 2016). For example, larger light extinction coefficients will lead to more absorbed shortwave radiation, resulting in thicker mixed layers (Wang et al., 2019); reducing light extinction coefficients in clearwater lakes may deepen the

thermocline and generate a warmer mixed layer (Wu et al., 2020). Previous studies on modifying the light extinction coefficient were primarily based on empirical estimations that neglected the seasonal fluctuation of lake water clarity caused by phytoplankton growth (Shatwell et al., 2016).

Lake Qiandaohu is located in the hilly areas of Zhejiang Province in eastern China. It has a complex morphology and remains thermally stratified throughout the year. Lake Qiandaohu is a warm monomictic lake and experiences short-term mixing in winter or spring (Zhang et al., 2014). Thermal stratification in Lake Qiandaohu usually begins in March and becomes the most intense in August and lasts until December, with a temperature difference between the surface and bottom ranging from 5 °C to 20 °C (Liu et al., 2019; Zhang et al., 2014). Although the phenology of its stratification has been well documented, the influencing mechanisms and evolution of lake physical characteristics (e.g. the water clarity and mixing process) are not clear. Proper parameterization in simulating the stratification in Lake Qiandaohu, as a representative of deep and warm monomictic lakes, would help to understand the evolution of the lake thermal structure. This study aims to: (1) improve the fundamental understanding of the thermal structure of Lake Qiandaohu, (2) address the influencing mechanism of key model parameters, and (3) provide references for WRF-Lake application in deep lakes. To achieve these goals, six sensitivity experiments were conducted in Lake Qiandaohu in 2016. This paper is organized as follows: Section 2 describes the WRF-Lake model configuration and numerical

158 experiments, and simulation results are presented in Section 3 and interpreted in
159 Section 4. The major findings of this study are presented in Section 5.
160
161 **2. Numerical modeling and simulation**
162 **2.1. Site description**
163 Lake Qiandaohu (29.37–29.83 °N, 118.57–119.25 °E) is a deep reservoir in
164 eastern China and means “thousand island archipelagoes” in Chinese; it was
165 established in 1959. It is a nationally protected drinking water source, with a basin
166 area of 10480 km^2 and a water volume of 178.4×10^8 m^3 when the normal water
167 storage water level is 108 m (Zhang et al., 2014). It has a water surface area of 580
168 km^2 with a length and width of 150 km and 50 km, respectively, at its widest point
169 (Zhang et al., 2014). Lake Qiandaohu is morphologically complex and contains five
170 sub-basins, the deepest of which is 105 m, although the average depth of the lake is
171 only 30 m (Zhang et al., 2014).
172 **2.2. WRF model configurations**
173 The Weather Research and Forecasting model version 4.0 (hereafter referred to
174 as “WRF”) (https://www2.mmm.ucar.edu/wrf/users) is a state-of-the-art numerical
175 weather prediction model. It solves the fully compressible Euler non-hydrostatic
176 equations using the Arakawa-C staggered grid, second- or third-order Runge-Kutta
177 time integration scheme, and terrain-following vertical coordinate system (Skamarock
178 et al., 2019).

In this study, the WRF model was configured with two one-way nested domains with horizontal resolutions of 5 km and 1 km, centered on Lake Qiandaohu (Figure 1), with 33 levels in the vertical direction. The selection of horizontal spacing considers both the computational efficiency and complex shape of Lake Qiandaohu. After several tests, the Yonsei University (YSU) planetary boundary layer scheme (Hong et al., 2006) and topographic correction method proposed by Jiménez and Dudhia (2012) were chosen to reach the minimum bias of wind speed. The Betts-Miller-Janjic cumulus convection scheme (Janjic, 1994) was applied to the outer 5 km resolution domain only. The Noah land surface scheme (Chen and Dudhia, 2001), WSM6 microphysics scheme (Lim and Hong, 2006), revised MM5 surface layer scheme (Jiménez et al., 2012) and UCM urban surface scheme (Chen et al., 2011) are also affiliated. To improve the atmospheric simulation, the temperature, humidity, and horizontal wind fields above the planetary boundary layer of the outer domain were nudged to the ERA5 reanalysis by employing analysis nudging (Stauffer and Seaman, 1994).

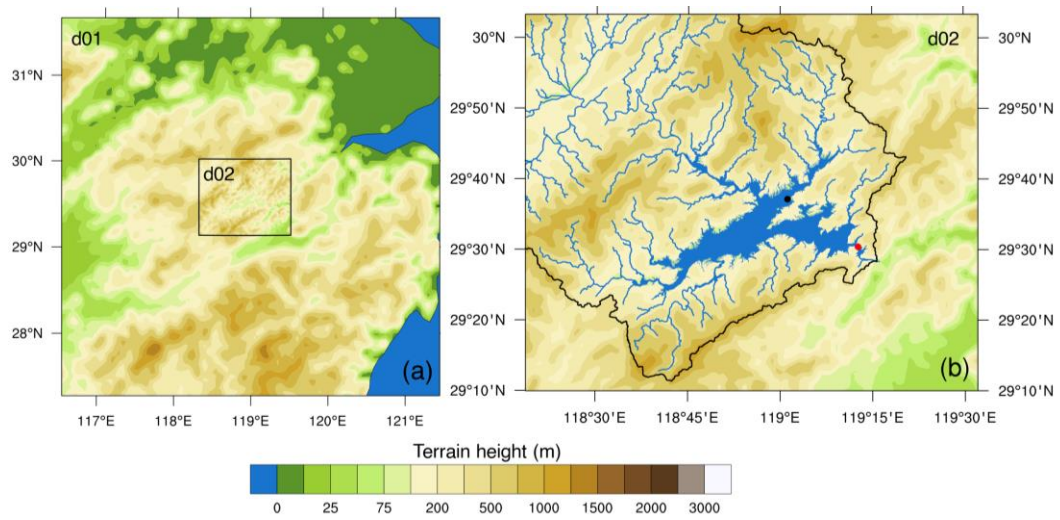

Figure 1. (a) Simulation domain with terrain height (m). The inner (1 km) grids are outlined in black. (b) Inner WRF grid and terrain height (m). The black dot and red dot in (b) denote the location of the Chun'an weather station and Daba buoy, respectively.

2.3. Simulating lake processes using WRF-Lake

2.3.1. Lake scheme of WRF-Lake

The lake scheme of WRF-Lake was derived from CLM 3.5, which was embedded into the WRF model (Gu et al., 2015). WRF-Lake is a 1D advection-diffusion lake model that discretizes the water column vertically into 0–5 snow layers, 10 water/ice layers, and 10 soil layers. The layer thickness of the first water/ice layer is always set to 10 cm and the other layer thickness is adjusted with fixed proportion. Taking the location of the Daba buoy as an example (~ 93 m), the layer depths (m) for the ten water/ice layers are listed as follows: 0.05, 4.75, 14.05, 23.35, 32.65, 41.95, 51.25, 60.55, 69.85, 79.15. The layer thickness is 0.1 m for the first layer and 9.3 m for the rest. We also performed numerical experiments using a 25-layer discretization scheme (as a grid-independence check, see Supporting Information 2). We found that although the 25-layer scheme generated smoother vertical water temperature profiles, the overall pattern of lake thermal structure was similar to that of the ten-layer one. Variations in lake water level and area are not considered in WRF-Lake.

The exchange of heat, moisture and momentum between the lake and overlying atmosphere is governed by the energy budget equation (Oleson et al., 2004) as:

$$\beta\vec{S}_g - \vec{L}_g - SH_{\uparrow} - LH_{\uparrow} - G_{\downarrow} = 0 \quad (1)$$

$$\vec{S}_g = (1-\alpha)SW_{\downarrow} \quad (2)$$

$$\vec{L}_g = \varepsilon\sigma T_g^4 - LW_{\downarrow} \quad (3)$$

where $\beta = 0.4$ is the fraction of the solar radiation absorbed at the lake surface; $\vec{S}_g$ is the net shortwave radiation (W m^{-2}); $\vec{L}_g$ is the net emitted longwave radiation (W m^{-2}); $SH_{\uparrow}$ is the turbulent flux of sensible heat (W m^{-2}); $LH_{\uparrow}$ is the turbulent flux of latent heat (W m^{-2}); $G_{\downarrow}$ is the net heat flux into the ground (W m^{-2}); α is the lake surface albedo; $SW_{\downarrow}$ is the downward shortwave radiation (W m^{-2}); $\varepsilon = 0.97$ is the lake surface emissivity; $\sigma = 5.67 \times 10^{-8}$ W m^{-2} K^{-4} (Stefan-Boltzmann constant); T_g is the lake surface temperature (K); and $LW_{\downarrow}$ is the downward atmospheric longwave radiation (W m^{-2}). Eqn. (1) is solved numerically by the Newton-Raphson iteration method to derive T_g and turbulent fluxes.

Subsurface energy transport is governed by the 1D heat diffusion equation (Hostetler and Bartlein, 1990; Oleson et al., 2004) and is expressed as follows:

$$\frac{\partial T}{\partial t} = \frac{\partial}{\partial z}\left[(k_m + k_e)\frac{\partial T}{\partial z}\right] - \frac{1}{c_w}\frac{d\phi}{dz} \quad (4)$$

where T is the lake temperature (K), t is time (s), $k_m = 1.43 \times 10^{-7}$ m^2 s^{-1} is the molecular diffusion coefficient, k_e is the eddy diffusion coefficient (m^2 s^{-1}), c_w is the volumetric heat capacity (J m^{-3} K^{-1}), and $\phi = (1-\beta)\vec{S}_g \exp^{-\eta(max(z-z_s,0))}$ is the solar radiation (W m^{-2}) penetrating to depth z (m); where $\eta = 1.1925d^{-0.424}$ is the light extinction coefficient (m^{-1}) as a function of lake depth d (m), and $z_s = 0.6$ m is the thickness of the surface layer.

In WRF-Lake, the mixing process is described using an advection-diffusion model (Eqn. 4), whereby the eddy diffusion coefficient k_e for layer i was calculated from the wind speed as described by Oleson et al. (2004):

$$k_{e,i} = \begin{cases} \frac{kw^* z_i}{P_0(1+37Ri^2)} \exp(-k^* z_i) & , T_g > T_f \\ 0 & , T_g \leq T_f \end{cases} \quad (5)$$

where $k = 0.4$ is the Von Karman constant; $w^* = 0.0012u_2$ is the surface friction velocity (m s^{-1}), where $u_2 = min(\frac{u_*}{k} ln(\frac{2}{z_{0m}}), 0.1)$ is the 2-m wind speed (m s^{-1}) calculated; z_i is the node depth (m); $P_0 = 1$ is the neutral value of the turbulent Prandtl number; R_i is the Richardson number given below; and k^* varies with latitude φ as $k^* = 6.6u_2^{-1.84}\sqrt{|\sin\varphi|}$.

The Richardson number R_i is defined as:

$$R_i = \frac{-1 + \sqrt{1 + \frac{40N^2k^2z_i^2}{w^{*2}\exp(-2k^*z_i)}}}{20} \quad (6)$$

where N^2 is the buoyancy frequency (s^{-2})

$$N^2 = \frac{g}{\rho_i}\frac{\partial\rho}{\partial z} \quad (7)$$

where g is the acceleration due to gravity and ρ_i is the density of water (kg m^{-3}).

2.3.2. Eddy diffusivity calculation from in situ measurements

The flux gradient method can be used to determine the eddy diffusivity k_e from in situ temperature measurements by integrating Eqn. (4) from depth z to the lake bottom at depth d while assuming that the turbulent heat flux and net radiation at the lake bottom are equal to zero (Powell and Jassby, 1974). Thus, k_e can be derived explicitly from the following expression:

$$k_e(z) = \left(\int_z^d \frac{\partial T}{\partial t} dz - \frac{1}{c_w} \phi(z) \right) / \frac{-\partial T}{\partial z} - k_m \quad (8)$$

where ϕ is calculated consistent with the procedure used in WRF-Lake.

Eqn. (8) is valid only below the mixed layer, where the heat transfer caused by convective mixing and horizontal advection can be neglected (Powell and Jassby, 1974). The 30-day averages of the lake water temperature and ϕ were used to estimate k_e at the center of this time interval. The 30-day averaging was used to smooth the profiles of k_e to better illustrate its variation with depth and time. Central-difference and forward-difference approximations were used for the spatial and time derivatives with Δz = 0.5 m and Δt = 30 days, respectively. The trapezoidal rule was applied for approximating the integral with a 0.5 m subinterval. Negative values due to cooling of the water column or unstable water layers are excluded from the results.

2.4. Improvements to the WRF-Lake model

2.4.1. Initial lake water temperature profile

The default initial lake water temperature in the WRF-Lake was derived from the ground temperature T_g as follows:

$$T_i = \begin{cases} T_g & , i = 1 \\ T_g + \dfrac{z_i(277 - T_g)}{50} & , z_i \le 50 \\ 277 & , z_i > 50 \end{cases} \quad (9)$$

Where the layer $i = 1$ denotes the top layer. We note that Eqn. (8) was derived from the observed lake temperature profile of Lake Superior. In the simulation results using the default lake scheme, the initialization procedure generated a large surface-bottom water temperature difference of 8.53 ℃, which is substantially higher than the

observed data (2.29 ℃). Overestimation of the initial lake water temperature gradients resulted in unrealistic cold biases for the lake bottom water temperature throughout the year. For lakes that regularly experience complete turnover, it can be assumed that the lake is fully mixed with a homogeneous temperature profile as the initial condition (Wu et al., 2020). However, Lake Qiandaohu is a monomictic lake with thermal stratification for most of the year, and the temperature gradient shift caused by the default lake scheme or a uniform initial profile cannot be easily corrected during model integration (Perroud et al., 2009). In this study, a straightforward and generalized method was proposed to assign initial values for lake temperature. WRF-Lake was modified to import lake water temperature profiles directly from external files and interpolate them onto the lake grid of the WRF model. We first replaced the lake depths in WRF with the observed bathymetry data. During the model initialization, each water column at lake grids will be discretized into ten layers according to their lake depths. Then we linearly interpolated the temperature profile at Daba to all grids to generate initial conditions for the entire simulation domain. This procedure assumes that the water temperature in Lake Qiandaohu is horizontally homogenous. The measurement depths at Daba are also adequate for providing water temperature profiles for other lake grids. The soil temperature was set equal to the lake water temperature of the bottom layer to ensure that the sediment heat flux was initially zero. Figure 2a depicts the default initial lake water temperature profile in WRF-Lake, observed values, and modified initial lake water temperature profile at the

Daba station (0000 UTC on 1st March 2016).

2.4.2. Time-dependent light extinction coefficient

The light extinction coefficient describes the rate at which the incident shortwave radiation is attenuated by lake water, which determines the vertical distribution of solar radiation. In the default WRF-Lake model, the light extinction coefficient was calculated as a function of lake depth (Section 2.3.1) using in situ observations from 88 Swedish lakes, which cannot be generalized to global lakes (Subin et al., 2012). The light extinction coefficient at the Daba station, for example, varies between 0.3–0.6 throughout the year, with the highest values in spring and summer; however, the default values in WRF-Lake remain constant and understated (Figure 2b). Therefore, the in situ observed monthly light extinction coefficients of Lake Qiandaohu were taken as model inputs and disaggregated to daily resolution during the simulation period, which accounted for the temporal variability of the light extinction coefficient.

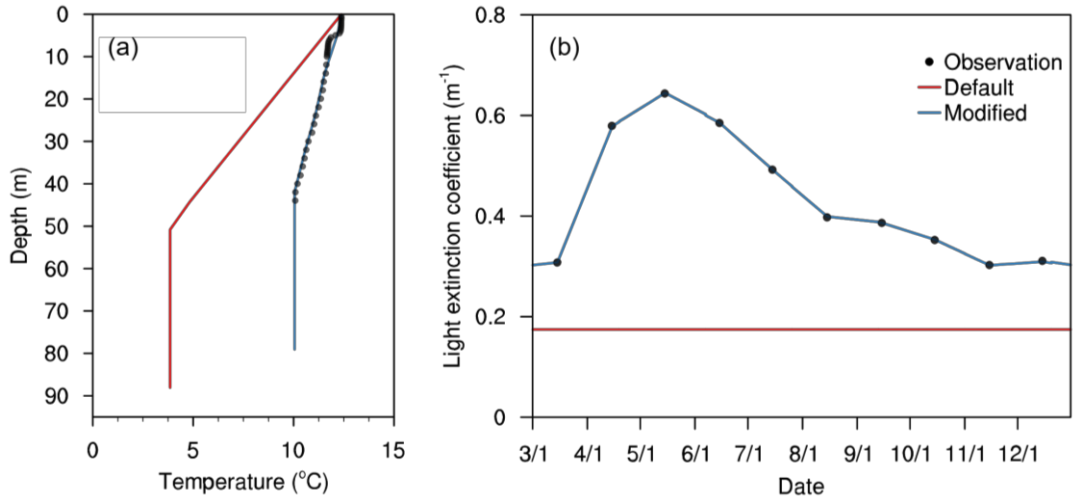

Figure 2. (a) Initial water temperature profile at Daba station from the observations, default, and modified lake scheme; (b) Monthly light extinction coefficients from

sampling and daily light extinction coefficients from the default and modified lake scheme.

2.4.3. Eddy diffusion coefficient

The governing equation of the heat transfer in the WRF-Lake was controlled by molecular diffusion and eddy diffusion. Gu et al. (2015) proved that the model performance for lake temperature was sensitive to eddy diffusion and could be improved by enlarging the eddy diffusivity (k_e) for deep lakes. The default lake model increased k_e by a factor of 100 when the depth of the lake grid exceeded 15 m. In this study, the factor was enlarged to 10^4 and restricted the total heat diffusion coefficient ($k_m + k_e$) with a maximum value of 0.01 m^2 s^{-1} to avoid unrealistic large diffusivity that may occur at the lake surface. This criterion is the largest vertical heat diffusivity observed in the open seas, as suggested by Wang et al. (2019).

2.4.4. Surface roughness lengths parameterization

The surface roughness length of momentum, sensible heat, and latent heat for unfrozen lakes is defined as 0.001 m in the default WRF-Lake, which can be considered excessive for lakes. The method proposed by Subin et al. (2012) was adopted is this study. It calculates the surface roughness lengths based on the friction velocity, fetch, and wind speed as follows:

$$\begin{aligned} z_{0m} &= max\left(\frac{0.1v}{u_*}, \alpha\frac{u_*^2}{g}\right) \geq 10^{-5}\text{m}, \\ z_{0h} &= z_{0m}\exp\left\{-\frac{\kappa}{P_r}\left(4\sqrt{R_0}-3.2\right)\right\} \geq 10^{-5}\text{m}, \\ z_{0q} &= z_{0m}\exp\left\{-\frac{\kappa}{S_c}\left(4\sqrt{R_0}-4.2\right)\right\} \geq 10^{-5}\text{m}, \end{aligned} \tag{10}$$

where v is the kinematic viscosity of air ($m^2\ s^{-1}$), u_* is the friction velocity ($m\ s^{-1}$), α is the effective Charnock coefficient (given below), $R_0 = max(\frac{z_{0m}u_*}{v}, 0.1)$ is the near-surface atmospheric roughness Reynolds number, $P_r = 0.71$ is the molecular Prandt number for air, and $S_c = 0.66$ is the molecular Schmidt number for water in the air.

The Charnock coefficient is defined as follows:

$$\begin{aligned} \alpha &= \alpha_{min} + (\alpha_{max} - \alpha_{min})\exp[-min(A, B)] \\ A &= \left(\frac{Fg}{u_*^2}\right)^{1/3} / f_c \\ B &= \epsilon \frac{\sqrt{dg}}{u} \end{aligned} \tag{11}$$

where $\alpha_{min} = 0.01$; α_{max}=0.11; F is the lake fetch (m); and f_c was set to 22, which corresponds to the use of u_* instead of u when calculating A (Wang et al., 2019); $\epsilon = 1$. The fixed-point iteration method proposed by Wang et al. (2019) was also used to update surface roughness lengths and u_* simultaneously.

2.5. Datasets

2.5.1. Reanalysis datasets

The initial and boundary conditions of the WRF model were provided by the 6-hourly ERA5 reanalysis (Hersbach et al., 2020) data with 1° spatial resolution. This is the latest fifth generation of atmospheric reanalysis dataset produced by the European Center for Medium-Range Weather Forecasts and has been applied widely in lake research (https://www.ecmwf.int/en/forecasts/datasets/reanalysis-datasets/era5).

The China Meteorological Forcing Dataset (CMFD) is a gridded near-surface meteorological dataset with a 0.1° spatial resolution and a three hour temporal

resolution (https://data.tpdc.ac.cn/en/data/8028b944-daaa-4511-8769-965612652c49). It is developed by combining remote sensing data, reanalysis datasets, and in situ measurements (He et al., 2020; Yang et al., 2010). It has been widely used in other lake modeling studies in China (Wang et al., 2019; Wu et al., 2020). Downward shortwave radiation and longwave radiation from this dataset were used as references to check the performance of the WRF model since the Chun'an weather station does not observe radiation components. CMFD has been used as a representative of observation for assessing other forcing data (Qi et al., 2022); its shortwave radiation has also been proven to be reliable for China (Yang et al., 2017). Despite that, some studies in Lake Namco have found inconsistencies between CMFD and in situ observations (Huang et al., 2019; Shi et al., 2022; Wu et al., 2021). To reduce the uncertainties caused by single forcing data, we also included the ERA5 reanalysis as a reference when validating the simulated longwave and shortwave radiations.

2.5.2 Meteorological observation

Daily observations of meteorological variables, including 2-m temperature, 10-m wind speed, and precipitation at the Chun'an weather station (29.62 °N, 119.02 °E) during 2016, were applied to evaluate the performance of the WRF model in simulating near-surface variables. Data were downloaded from the China Meteorological Data Service Center (http://data.cma.cn).

2.5.3 Lake water temperature observation in Lake Qiandaohu

In-situ lake water temperature measurements at the Daba buoy station in 2016

(29.51 °N, 119.21 °E; hereafter referred to as "Daba") are used to calibrate model parameters. The water temperature was recorded every three hours by a multiparameter water-column profiler attached to a buoy. Vertical depths (± 0.005%) and water temperature (± 0.002%) were sampled at 0.5 m intervals between 0.1–10 m, and 2 m depth increments were used below 10 m (Liu et al., 2019). This sampling location had a maximum depth of 93 m. But the records only reached 65 m because the water temperature is vertically homogenous down below (Liu et al., 2019). For the convenience of cross-comparison, the water temperature from both in situ observations and numerical experiments was interpolated to 0.5 m intervals from 0.5–64 m.

2.5.4. Light extinction coefficient measurements

Light extinction coefficients η (m^{-1}) were obtained from monthly sampling of water transparency z_{secchi} (m) measured by the Secchi disk method. In this study, light attenuation was calculated using the relationship $\eta = 1.3809 z_{secchi}^{-0.92}$, which was estimated from a series of concurrent observations of z_{secchi} and light absorption (Figure S5).

2.6. Metrics of stratification and mixing

The lake analyzer (https://gleon.org/research/projects/lake-analyzer) is a numerical code package for calculating the key metrics of lake physical states from water temperature, lake bathymetry, and near-surface wind speed (Read et al., 2011). Three indicators were selected to represent the lake thermal structure characteristics

during stratification: the thermocline depth (thermD), thickness of the metalimnion (metaTh), and bottom depth of the metalimnion (metaB). ThermD was defined as the depth of the maximum change in water density. The metalimnion range is defined as the water layer where the vertical temperature gradient is $\geq 0.2\ ℃\,m^{-1}$ (Liu et al., 2019; Zhang et al., 2014). Schmidt stability, which denotes the resistance of mechanical mixing because of potential energy, was also calculated to represent the temporal variation of lake thermal stability (Schmidt, 1928). The lake number and Wedderburn number were calculated to describe the dynamic stability. The two dimensionless metrics are expressed as the balance of wind stress and the stratified condition. Lake number represents the potential for nonlinear internal waves caused by wind forcing (Imberger and Patterson, 1989). Meanwhile, the Wedderburn number, represents the possibility of upward movement in the metalimnion (Thompson, 1980). Lower lake number and Wedderburn number values indicate a higher likelihood of mixing events (Read et al., 2011).

2.7. Experimental design and post processing

Six numerical experiments were conducted to assess the impact of key parameters that individually affect the lake thermal structure and evaluate performance of the modified WRF-Lake model, as shown in the table below. Since lake temperature measurements below 30 m were not available from January to February 2016, all simulations ran from March 1, 2016, to January 1, 2017, and the

first 20 days were discarded as model spin-up.

Table 1. Model parameter setting for different cases.

Case	Description
CTL	Control experiment
INI	Modified initial lake temperature as described in Section 2.4.1
KD	Modified lake light extinction coefficient as described in Section 2.4.2
KE	Modified eddy diffusivity as described in Section 2.4.3
Z0MG	Modified surface roughness lengths as described in Section 2.4.4
MOD	Calibrated model based on INI, KD, KE, and Z0MG

In this study, the mean bias error (MBE) was used to represent systematic error of the lake model. This metric provides the average bias of a model in comparison to observations and indicates whether the model needs to be corrected. The root mean square error (RMSE) was used to assess the credibility of the model. This is the standard deviation of the predicted errors and is highly sensitive to the most significant errors.

3. Results

In this section, the results from the WRF-Lake simulations are first validated using in situ observations and other available datasets. After the sensitivity experiments, the lake water temperature and the sensible and latent heat fluxes are further analyzed to determine the effects of key model parameters on the lake surface energy balance and thermal structure.

3.1. Model validation

3.1.1 Comparison of meteorological variables

The simulated near-surface air temperature and wind speed from the control experiment were compared with those obtained from meteorological observations. Since radiation measurements from nearby weather stations were unavailable, the CMFD dataset was used as a reference to assess the accuracy of downward shortwave and longwave radiation, which act as the primary energy sources for the lake.

The WRF model accurately reproduced daily variations of 2-m air temperature, downward longwave radiation, and 2-m relative humidity, as well as the seasonal pattern of downward shortwave radiation and 10-m wind speed (Figure 3). The comparison of simulated spatial pattern between CTL and reanalysis dataset were shown in Figure S13-14. As shown in Figure 3 and Table 2, the temporal variations in air temperature and downward longwave radiation were captured well by the WRF with an MBE of 0.4 °C (− 0.6/-13.9 W m^{-2}; the comparison between WRF and ERA5/CMFD) and a RMSE of 1.3 °C (9.3/20.4 W m^{-2}). The WRF model underestimated relative humidity by an MBE of -1.5%. This is possibly related to the warm biases in air temperature, which results in larger saturated water vapor pressure. The WRF model was also able to simulate reasonably the daily variation in wind speed, although there is a large positive bias with an annual MBE of 2.7 m s^{-1} and an RMSE of 3.0 m s^{-1}. This indicates a systematic overprediction of wind speed and the degree of which amplified at higher velocities. The simulated downward shortwave radiation was also overestimated, with a mean MBE of 82.0/84.7 W m^{-2}. Detailed

investigations of the overprediction of wind speed and shortwave radiation are not within the scope of this study. However, their effects on lake thermal structures are further discussed in Section 4.1.

Table 2. Annual mean bias error (MBE) and root mean square error (RMSE) of the WRF model simulation when compared with the observations (2-m air temperature, 10-m wind speed, and 2-m relative humidity) and reanalysis dataset (downward shortwave and longwave radiation).

	Reference data	MBE	RMSE
2-m air temperature (℃)	in situ	0.4	1.3
10-m wind speed (m s^{-1})	in situ	2.7	3.0
Downward longwave	ERA5	–0.6	9.3
radiation (W m^{-2})	CMFD	-13.9	20.4
Downward shortwave	ERA5	82.0	95.8
radiation (W m^{-2})	CMFD	84.7	103.0
2-m relative humidity (%)	in situ	-1.5	7.0

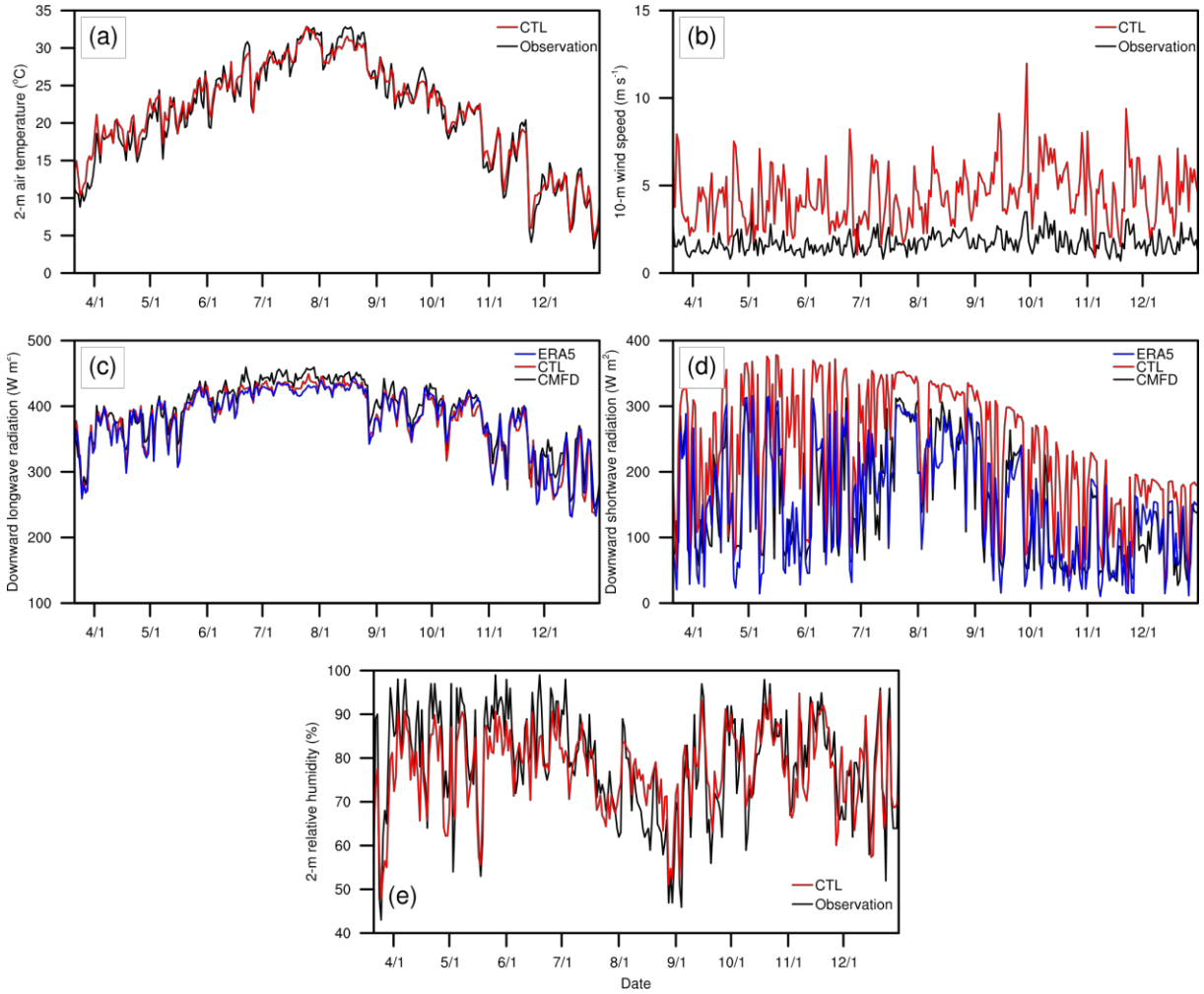

Figure 3. Daily variations in (a) 2-m air temperature (℃), (b) 10-m wind speed (m s^{-1}), (c) downward longwave radiation (W m^{-2}), (d) downward shortwave radiation (W m^{-2}), and (e) 2-m relative humidity (%). Air temperature, wind speed, and relative humidity are compared to the observations from the Chun'an weather station. Longwave and shortwave radiation are compared with those obtained from reanalysis datasets (i.e., CMFD and ERA5). All variables were interpolated from model grid cells to the Chun'an station.

3.1.2 Comparison of lake surface energy processes

LSWT is determined by heat exchange processes at the air–water interface,

namely, absorbed radiation, heat conduction, and heat loss by evaporation (Edinger et al., 1968). Since the net shortwave radiation and downward longwave radiation are subjected to atmospheric conditions, this section analyzes the LSWT and turbulent fluxes to determine effects of the model parameters on the lake surface energy processes. The emitted longwave radiation is not included because it is proportional to the fourth power of the absolute temperature (the first term on the right-hand side of Eqn. 3); thus, it varies naturally with LSWT.

LSWT in this study is the average water temperature between 0-2 m. The simulated data at 0400 UTC (12:00 in local time) each day were chosen for a stable and intense thermal stratification (Liu et al., 2019). The WRF-Lake results were interpolated to the location of Daba buoy to compare with the observations. Results of simulated LSWT, sensible and latent heat are shown in Figure 4 and Figure S6. The comparison of simulated spatial pattern between CTL and other experiments of lake water temperature at the top model layer was shown in Figure S15. Compared with in situ data, CTL successfully reproduced the seasonal variation of water temperature (Figure 4a), but significantly underestimated LSWT from September to December. This results in an annual MBE of –1.3 ℃, which indicates a systematic cold bias. In addition, CTL simulated excessive variation in LSWT, particularly during the warming period (March–June), with an average of 1.7 ℃. It is still comparable to the daily variation in air temperature (1.7 ℃) but considerably higher than the observed daily variation in water temperature (0.5 ℃).

CTL generated a reasonable temporal pattern of turbulent heat fluxes at the lake surface. Figure 4b shows that the latent heat flux exhibited an increasing trend before September and reached its peak in autumn because of the lag between the LSWT and air temperature (Schmid and Read, 2021). This is consistent with the enhanced sensible heat flux since August (Figure 4c) and implies that the lake surface is warmer than the overlying atmosphere and serves as a heat source. Figures 4b and 4c also highlight the dominant contribution of evaporation to turbulent heat fluxes, as is expected in low-latitude lakes such as Lake Qiandaohu (Woolway et al., 2018).

As indicated by the RMSE and MBE (Figure 5), all five parameter sensitivity experiments improved the accuracy of LSWT except INI, which exacerbated the cold biases. Results with increased light extinction coefficient warmed the water surface during most of the simulation period (93.4%), consequently yielding a 0.4 ℃ increase in annual MBE. The INI experiment corrected the overestimation of LSWT at the beginning of the simulation. The difference between INI and CTL diminished until November, when INI began to display a negative bias against CTL and eventually resulted in a decrease in annual MBE of 0.1 °C. The only experiment with a positive MBE of 0.1 °C against observation was Z0MG. This matched the minimum latent heat flux generated by Z0MG in the five sensitivity experiments (Figure 4b). Despite an increase of 1.1 W m^{-2} in the annual average sensible heat flux of Z0MG, the latent heat flux decreased by 14.0 W m^{-2} because of less effective moisture exchange at the air–water interface and dominated changes in LSWT. Enlarging the eddy diffusivity in

514 the deep layers mitigated the cold bias of the LSWT from October to December,
515 which was analogous to Z0MG. However, for the other months of the year, KE
516 estimated colder LSWT than CTL.

517 After the calibrations, the MOD experiment achieved a minimum MBE of –0.1 ℃
518 and lowered the RMSE from 2.9 ℃ to 1.6 ℃. The remaining cold bias was partially
519 because of the positive bias in the near-surface wind speed introduced by the WRF
520 model (Figure 3b). Windier conditions promote stronger mixing events in the
521 epilimnion and favor turbulent heat loss (especially latent heat) at the air–water
522 interface, thereby resulting in a cooling effect on LSWT (Woolway et al., 2018).

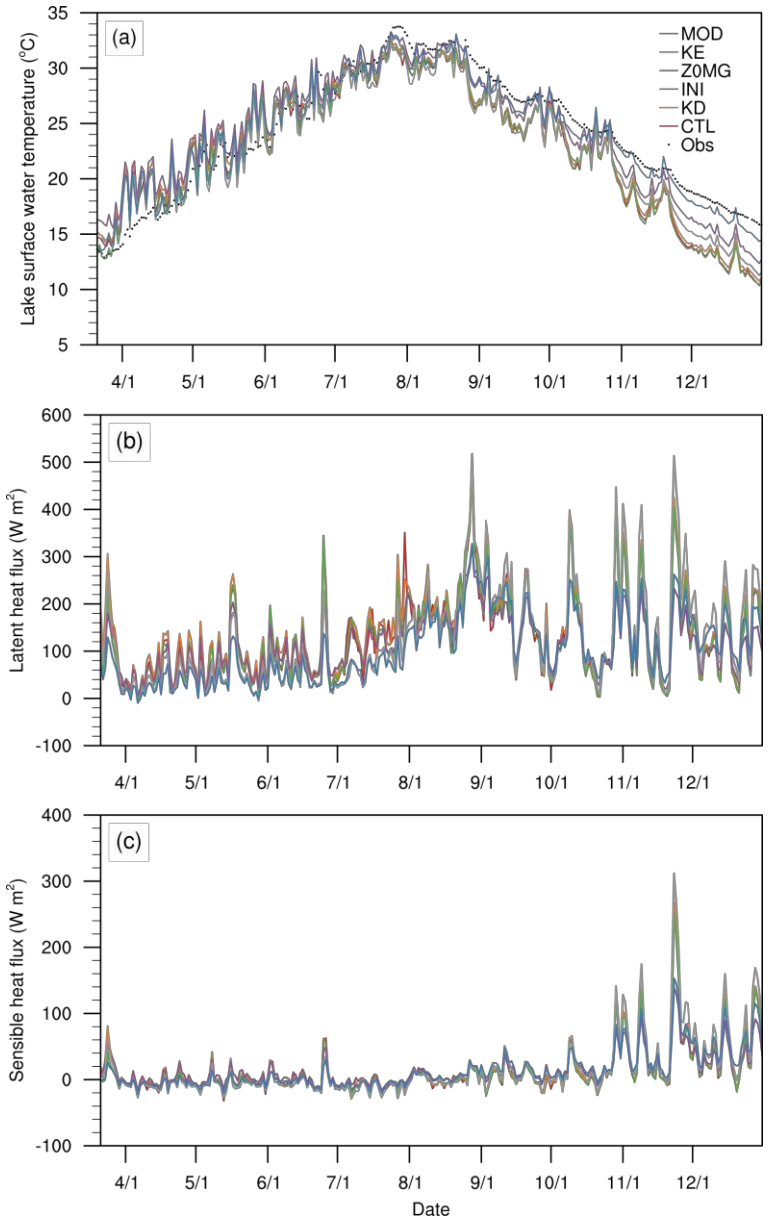

523

524 Figure 4. Daily variation of (a) lake surface water temperature (℃), (b) sensible heat

525 flux (W m^{-2}), and (c) latent heat flux (W m^{-2})

526

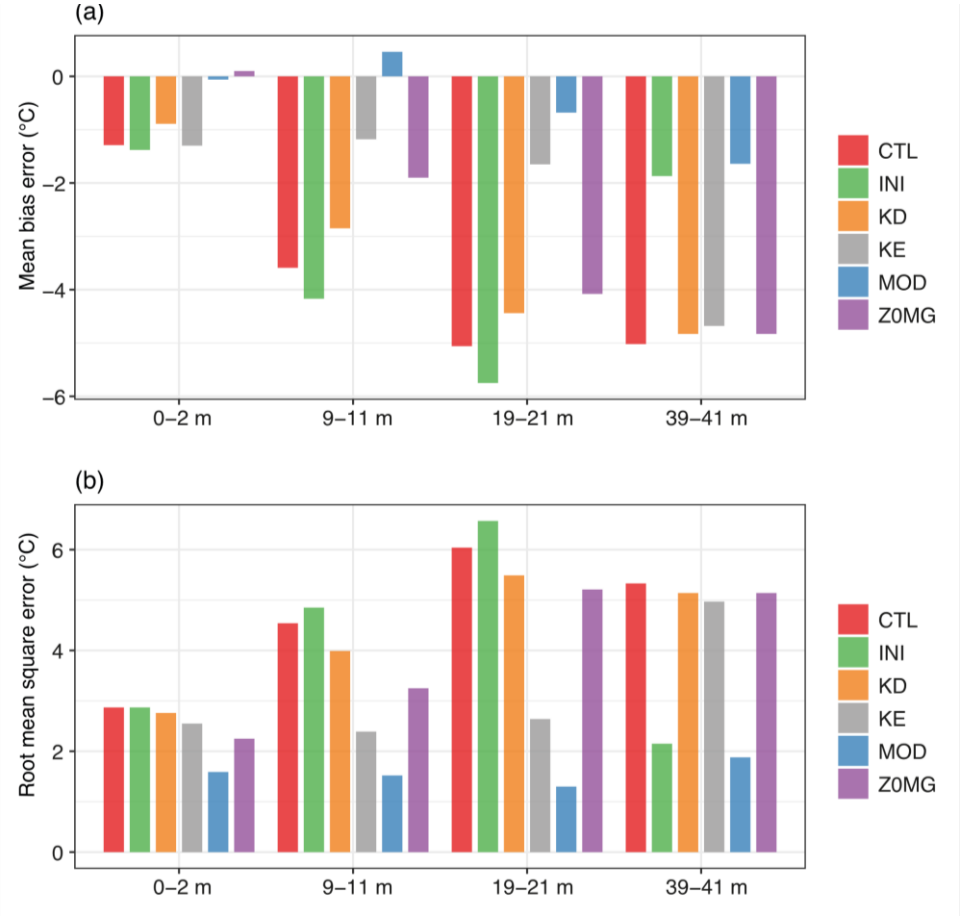

Figure 5. (a) Mean bias error (℃) and (b) root mean square error (℃) for 0–2 m, 9–11m, 19–21 m, and 39–41 m averaged water temperature between the simulation results and observations.

3.2. Simulating stratification in Lake Qiandaohu

Results of the CTL experiment showed that the original lake scheme could represent the temporal evolution of lake stratification. Lake thermal stratification began in March and strengthened rapidly in April, with the temperature difference between the surface and bottom of the lake (hereafter denoted as T_{diff}) exceeding 5 ℃ on April 2. Further, lake stratification was found to be strongest during summer, when the temperature difference reached 23.4 ℃ on July 26 (Figure 6a). CTL captured this feature relatively well, with the maximum temperature difference occurring on July

539 25 (Figure 6b). However, CTL predicted an earlier spring warm-up and autumn cool-
540 down. The hypolimnion temperature was severely underestimated, which results in an
541 unrealistic vertical temperature gradient in the deep layers. This also caused the
542 maximum T_{diff} of the CTL experiment to be 6 ℃ higher than that observed. Moreover,
543 the default lake scheme generated weaker lake stratification, which is indicated by the
544 negative annual MBE of the thickness of the metalimnion in the INI experiment
545 (Figure 10). It is noteworthy that the positive systematic error of the metalimnion
546 bottom depth and metalimnion thickness in CTL was attributable to overestimation of
547 the initial hypolimnion temperatures.

548 As shown in Figure 6, the lake temperature simulated by KD and Z0MG were
549 very close to that of CTL. Although the hypolimnion temperature in the INI
550 experiment was more accurate, it simulated a metalimnion structure that was very
551 similar to that of CTL, which was greatly improved in the KE experiment. These
552 results confirm that the vertical heat distribution is primarily governed by the mixing
553 process (Subin et al., 2012). Modifying surface properties of the lake (such as surface
554 roughness lengths and light extinction coefficient) has limited effects on the vertical
555 temperature pattern (Xiao et al., 2016).

556 Figure 7 and Figure S10 showed the differences in the temperature simulated
557 from all the sensitivity experiments against CTL and the observations, respectively.
558 The comparison of vertical water temperature profile was depicted in Figure S11. It
559 can be first noted that the KD and Z0MG were both close to CTL and showed an

560 overall warming trend in the whole water column. INI and KE showed the largest
561 deviation from CTL. An increase in the light extinction coefficient resulted in a
562 warming of the lake surface in early summer, as well as a water temperature of
563 approximately 15 m during stratification, leading to a temperature increase of 2.0 ℃.
564 Negative values only occurred at the lake surface for a few days, possibly because of
565 the increased latent heat flux (Figure 4c). The INI experiment removed cold bias
566 below 25 m. However, it tends to produce a warmer LSWT from June to October and
567 a colder metalimnion throughout the year, deteriorating the model performance at 9–
568 11 and 19–21 m (Figure 5). When a parameterization for surface roughness lengths
569 was used, the water column temperature increased by an average of 0.6 ℃ above 25 m.
570 The most pronounced improvements occur at 1–15 m in winter, which largely delayed
571 the earlier prediction of the autumn cool-down, although an even earlier warm-up was
572 estimated (Figure 6e). Enlarging the eddy diffusivity decreased the water temperature
573 above 5 m before September and increased the water temperature below it, thereby
574 implying that more heat energy was transferred to the deep layers by enhancing the
575 mixing strength. Warmer deep layers allow more energy to be stored below the mixed
576 layer, where the air–water heat exchange takes place. This further enhances the
577 resistance of the lake to declining air temperature, which is indicated by the warmer
578 water column in winter. These results suggested that, in addition to dominating the
579 development of the metalimnion, the mixing strength in the lake model influences the
580 thermal structure during the subsequent cool-down period. We have also performed a

numerical experiment with only the modified initial water temperature profile and eddy diffusivity (Figure S16 and Table S3). The results produced a similar thermal structure with MOD, but the water temperatures above 25 m were colder and showed larger biases. This suggests that the initial water temperature profile and eddy diffusivity were most critical for simulating the evolution of the lake thermal structure. At the same time, modifying light extinction coefficients and surface roughness lengths, which mainly increased water temperature in shallow layers, are important as well.

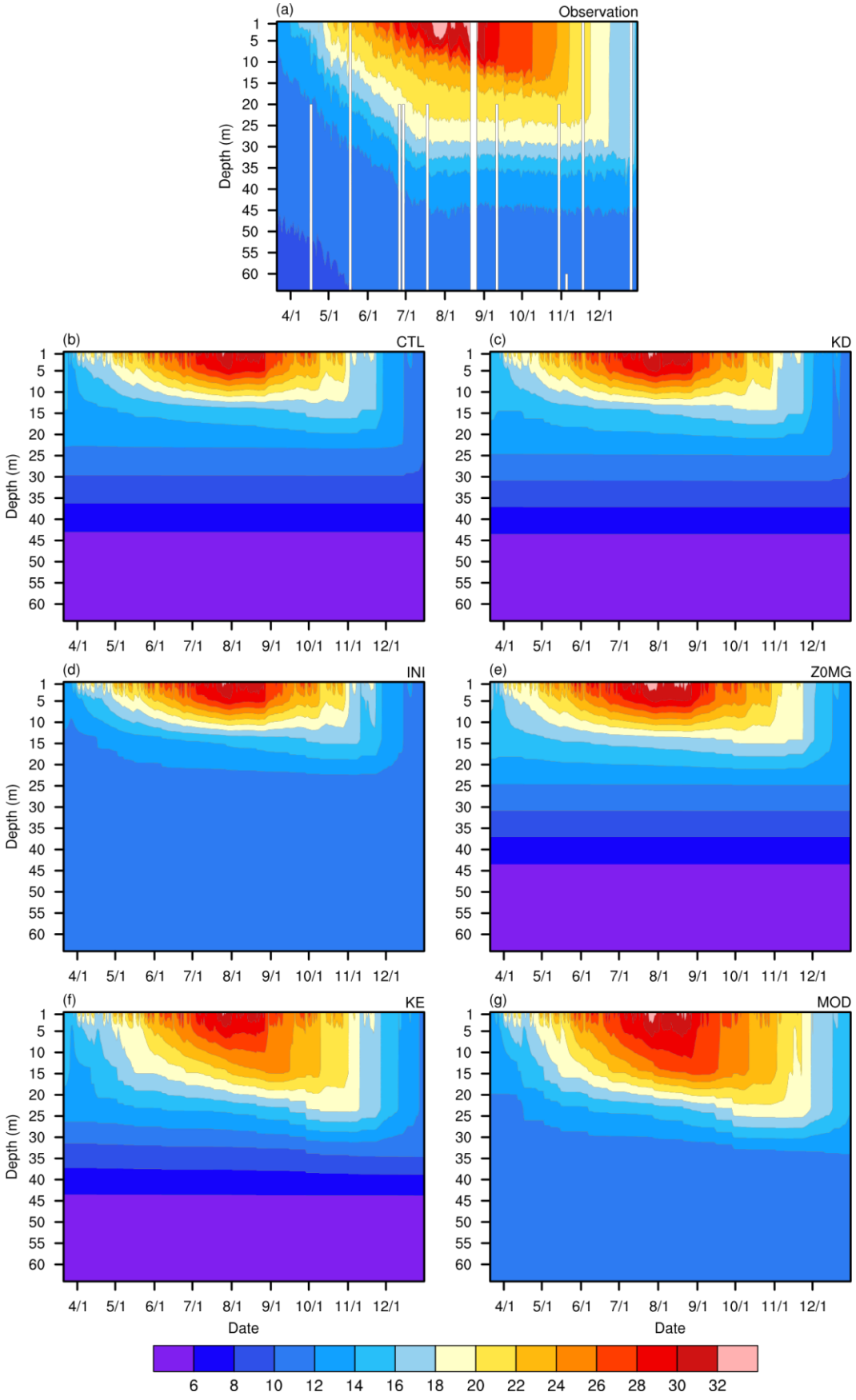

590

591 Figure 6. Lake water temperatures (℃) at the Daba station in 2016 (a) from

592 observations and as predicted by the lake models: (b) CTL, (c) KD, (d) INI, (e) Z0MG,

593 (f) KE, (g) MOD.

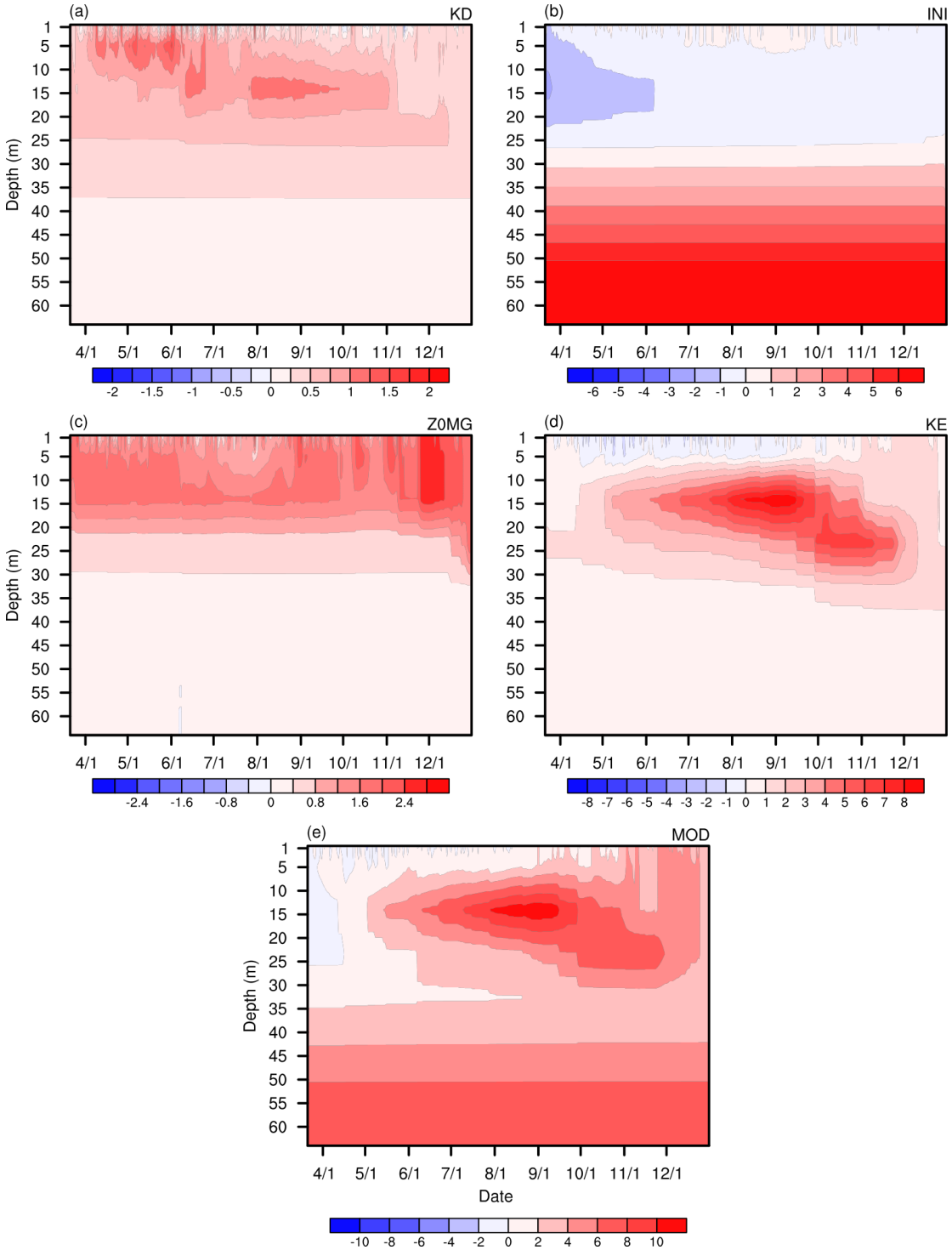

594

595 Figure 7. Differences between lake water temperatures (℃) simulated by (a) KD, (b)

596 INI, (c) Z0MG, (d) KE, and (e) MOD and CTL.

The performance of the MOD experiment in simulating water temperature at certain depths is shown in Figure 8. Figure 8 b–d denotes the water temperature at a depth of 9–11 m (above the thermocline), 19–21 m (below the thermocline), and 39–41 m (hypolimnion), respectively. In summary, accuracy of the lake scheme was greatly improved by modifying the aforementioned key model parameters, namely, the initial lake water temperature, light extinction coefficient, eddy diffusion coefficient and surface roughness lengths. The MOD experiment captured the seasonal variation and magnitudes of water temperature and reproduced the extended highest water temperature at 19–21 m compared to that at the surface. Nevertheless, the differences between the MOD and in situ measurements became apparent as the depth increased. Overestimation of water temperature at 9–11 m from June to August and underestimation in 19–21 m suggests insufficient heat transfer below the thermocline. The MOD experiment also failed to reproduce the slow warm-up of the hypolimnion temperatures, thereby implying unresolved mixing processes in the deep layers.

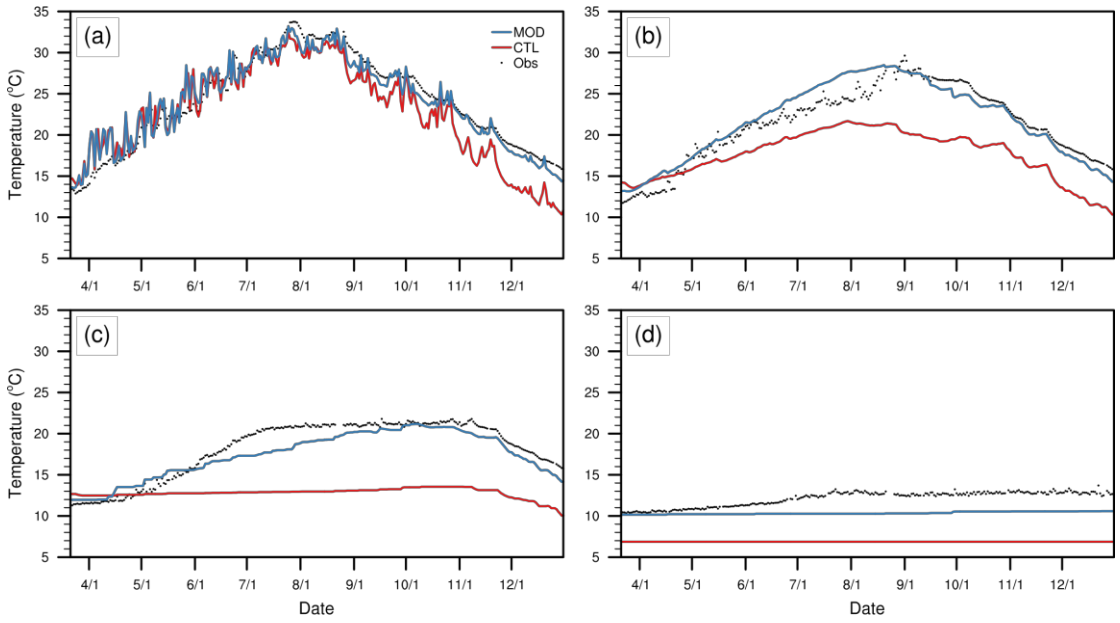

Figure 8. Temporal variation of daily water temperature (℃) at depths of (a) 0–2 m, (b) 9–11 m, (c) 19–21 m, and (d) 39–41 m from CTL and MOD simulations and in situ observations.

The temporal variations in the four modelled lake stability indicators calculated by Lake Analyzer were consistent with those calculated from the observations (Figure 9). Schmidt stability varies coherently with LSWT as it only depends on the water density (Figure 9a). The rising Schmidt stability before September suggested that the kinetic energy required to disturb lake stratification increased. Thermal stability weakened during the cooling period but still exceeded 1000 J m^{-2} in winter, which is reasonable for a deep and warm monomictic lake. The magnitude of the Schmidt stability in the MOD experiment was consistent with that of the observations, which was attributed to a better representation of the vertical heat content. Figure 9b shows that the thermocline depth changed rapidly in spring and gradually deepened with a

strengthening of summer stratification. During the cool-down period, the upper water column was fully mixed, and the thermocline depth was maintained near the bottom of the metalimnion. The MOD and CTL experiments both captured the sudden increase in thermocline depth in autumn, but failed to reproduce the steady growth behavior before that. The overestimation of wind speed and hypolimnetic water density resulted in lower lake numbers in the numerical experiments (Figure 9c). The lake number from the observations increased with Schmidt stability and the bottom layer depth of the metalimnion from April to July and then slowly decreased. For most of the year, the lake number from the observations remained above 10, which implies that wind forcing could only stir the uppermost layer of the lake and was incapable of diapycnal mixing (MacIntyre et al., 1999). Similar to the lake number, the Wedderburn numbers in the simulations were also underestimated owing to an overestimation of wind speed (Figure 9d). Variations in the Wedderburn number were primarily determined by changes in the mixed layer depth. In the CTL experiment, the mixed layer depth remained stable until November, which caused a downward trend in the Wedderburn number from August to October owing to the reduced density difference between the epilimnion and hypolimnion. However, the Wedderburn number increased with the mixed layer depth since September in the MOD experiment and observations. The Wedderburn number calculated from observations seldom fell below one, which suggests a low likelihood of upwelling events.

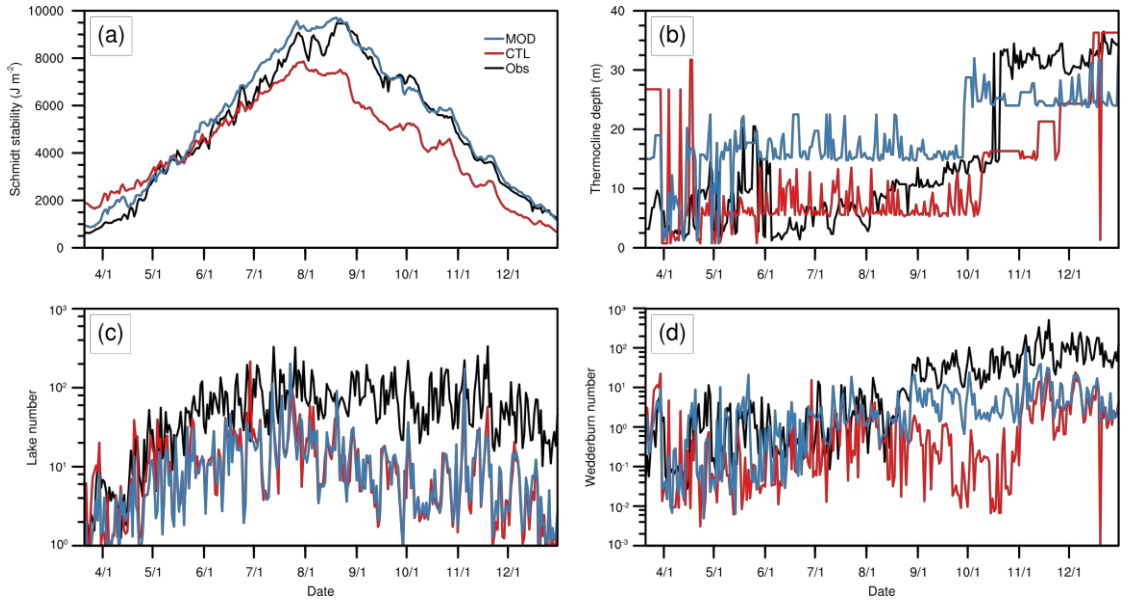

Figure 9. Temporal variation of daily (a) Schmidt stability (J m^{-2}), (b) thermocline depth (m), (c) lake number and (d) Wedderburn number from CTL and MOD simulations and in situ observations.

Figure 10 demonstrates the accuracy of the simulated thermal stratification by the annual MBE and RMSE of the thermal characteristics in the numerical experiments against observations. The MOD experiment improved the model performance in estimating metaTh and metaB and reduced the MBE to –2.2 m and –1.7 m, respectively. The remaining negative biases may be attributed to the weaker mixing strength below the thermocline (Figure 8 c–d). The ThermD estimated by the tuned model has an MBE of 1.0 m and an RMSE of 8.8 m, which is significantly better than that in large-scale simulations with uncalibrated models (Guo et al., 2021). The MOD experiment also improved the performance of the model in simulating the strength of summer stratification. The T_{diff} estimated by the MOD was 23.7 ℃

occurred on July 25, with 0.2 ℃ higher than that in observations and one day ahead.

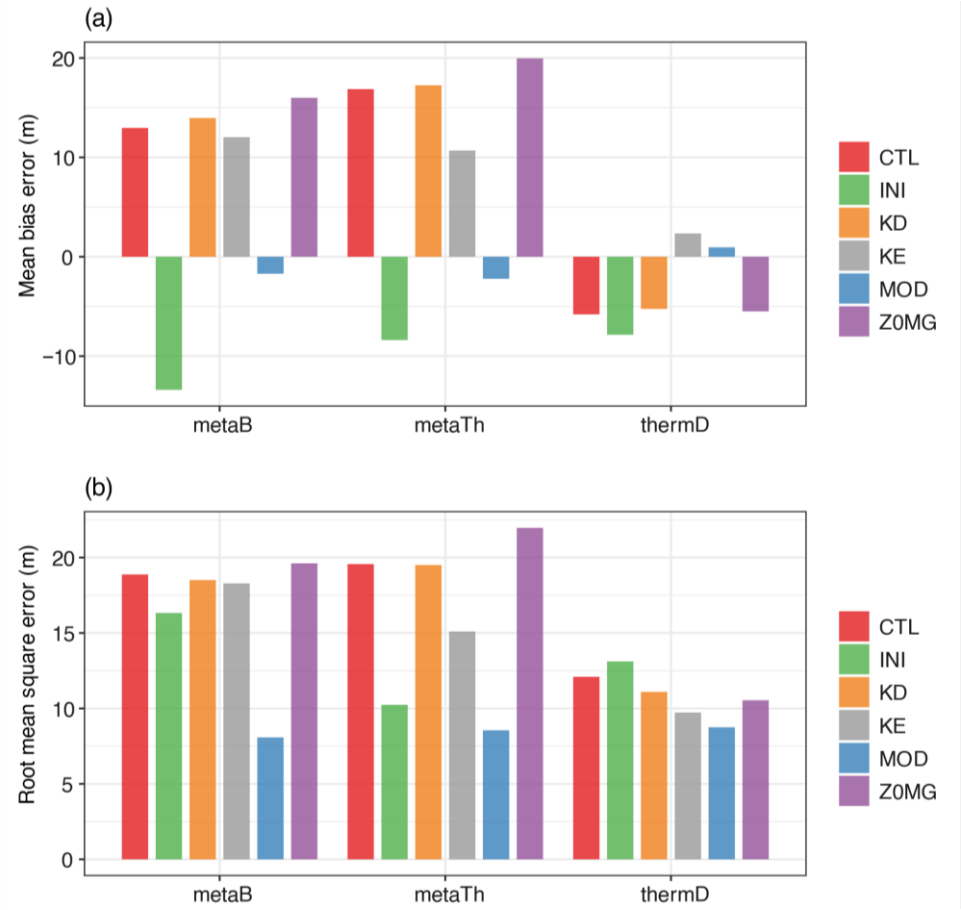

Figure 10. (a) Mean bias error (m) and (b) root mean square error (m) of simulated metalimnion bottom depth (metaB), metalimnion thickness (metaTh), and thermocline depth (thermD) against the observations.

3.3. Calculation and analyses of eddy diffusivity

k_e was computed from the observed water temperature using the approach described in Section 2.3.2 to quantitively evaluate the limitation of the Henderson-Sellers eddy diffusivity. It is noteworthy that k_e produced by Eqn. (14) is a proxy for all three-dimensional processes that contribute to turbulence in Lake Qiandaohu. Therefore, a similar variation pattern and magnitude of the tuned k_e were expected for

accurate simulation of the thermal structure.

Figure 11 depicts k_e computed from the observations (k_{eobs}) and the enlarged k_e in the MOD experiment (k_{emod}). The profiles of k_{emod} at different seasons were very similar. The k_{emod} first decreased markedly with increasing depth and reached its minimum in the 20–50 m depth range because of increasing vertical temperature gradients. Notably, the water temperature at deep layers was almost homogeneous in the vertical direction (Figure 6g; Figure S11), and the R_i in Eqn. (5) decreased from ~10^2 to zero (Figure S12) and therefore resulted in large k_{emod} comparable to that in shallow layers. This behavior suggests that WRF-Lake is also unable to simulate the vertical heat distribution in the hypolimnion, not only its temporal variation (Figure 8d), which is possibly related to the unresolved heat diffusion in the hypolimnion (see discussion in Section 4.2.3). It is evident that the profiles of k_{eobs} varied significantly with time and depth. The k_{eobs} values ranged from 1.3×10^{-8} to 3.0×10^{-4} m^2 s^{-1} with an average of 4.0×10^{-5} m^2 s^{-1}. This result is consistent with previous findings in Lake Zurich, another large and deep lake (Li, 1973). The highest k_{eobs} occurred in early summer (March–June), caused by the warming of the water column and the relatively weak vertical temperature gradient. After the stabilization of stratification in summer, the k_{eobs} rapidly declined because of the strong temperature gradient. In August, the k_{eobs} was negative at almost every depth except 7–12.5 m, where the warming trend lasted until September. This phenomenon is in line with the observed lagged maximum temperature in 9–11 m compared to that in 0–2 m from observations

(Figure 8a–b). The profiles of k_{eobs} in early summer showed a local minimum of k_{eobs} at approximately around 2.5 m, which corresponds to the depth of thermocline. The k_{eobs} further increased and formed a maximum at approximately 20 m. Below 20 m, the behavior of k_{eobs} varied largely with depth in different seasons. In March and April, k_{eobs} gradually decreases with depth from top to bottom. In the remaining months, however, the k_{eobs} formed a local minimum at 30–40 m, which is possibly related to the warm-up of water temperature at 39–41 m (Figure 8d). The minimums of the k_{eobs} profile matched the two gradient extremes in water temperature profile (Figure S7).

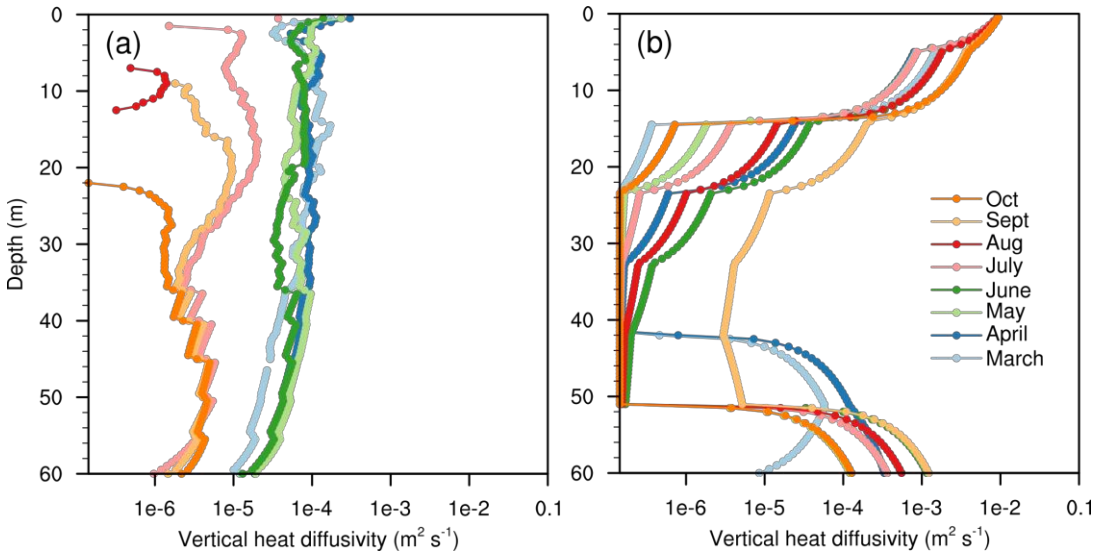

Figure 11. Vertical heat diffusivity (m^2 s^{-1}) (a) calculated from water temperature measurements and (b) simulated by the MOD experiment.

4. Discussion

This study aimed to simulate the temporal evolution of thermal stratification in a subtropical deep reservoir, Lake Qiandaohu, using an improved WRF-Lake model.

712 The results show that the improved model with the necessary parameterization can
713 capture variations in water temperature and intensity of lake stratification.

714 **4.1. Model uncertainty**

715 In a coupled system, the foremost concern is the error introduced by the
716 atmospheric model (in this case WRF) for simulating physical processes in the lake.
717 The 10-m wind speed and downward shortwave radiation were largely overestimated
718 by the model. The near-surface wind speed of the ERA5 reanalysis, which provided
719 initial and boundary conditions, showed a magnitude comparable to the observations
720 (Figure S8). This overprediction may be related to deficiencies in the WRF model.
721 WRF is deficient in representing the drag effect because of subgrid-scale orography
722 and tends to underestimate wind speed spatial variability over complex terrain
723 (Jiménez and Dudhia, 2012); thus, WRF overpredicts wind speed in valleys, where
724 Lake Qiandaohu is located (Figure 1b).

725 Positive error of the downward shortwave radiation simulated by the WRF model
726 is consistent with previous studies that evaluated the performance of atmospheric
727 models in representing surface energy fluxes. For example, the WRF model
728 overestimated shortwave radiation with an average MBE of 152.9 W m^{-2} compared to
729 those of the hourly observations in the Heihe River Basin (Pan and Li, 2011). The
730 biases of simulated surface insolation is caused by an inaccurate representation of the
731 radiation transfer process between the top of the atmosphere and ground (Wild, 2005).
732 This suggests that misrepresentations of cloud properties, rather than radiation

schemes, are responsible for these biases (Jousse et al., 2016). Studies at regional scales have also suggested that an overestimation of the downward shortwave radiation by WRF may be attributable to the lack of cumulus cloud amount and uncertainty in aerosol optical depth (Avolio et al., 2017; Kumar et al., 2015; Ruiz-Arias et al., 2016).

In the lake scheme, wind speed was used to calculate the friction velocity, which further influenced the simulated water temperature from two perspectives. First, the sensible and latent fluxes from Eqn. (1) are estimated using the bulk aerodynamic algorithm proposed by Zeng et al. (1998), where the surface fluxes of heat and water vapor are proportional to the friction velocity. Second, the 2-m wind speed in Eqn. (5) also varies with the friction velocity. Therefore, a higher wind speed promotes the efficiency of heat and water vapor exchange at the lake surface and enhances mixing strength in the subsurface (Woolway et al., 2021). Schmid et al. (2014) investigated sensitivity of the lake surface equilibrium temperature to climate forcing variables. According to these findings, overestimation of the average annual 10-m wind speed by 2.7 m s^{-1} (Table 2) will lead to a decrease in LSWT by 2.7 ℃. However, LSWT will simultaneously increase by 2.5–4.9 ℃ because of positive biases in solar radiation. Therefore, the effects of overestimated wind speed and downward shortwave radiation on LSWT may partially compensate for each other. The remaining cold bias in LSWT is presumably because of the favored turbulent heat loss (especially latent heat) under windy conditions (Woolway et al., 2018). Notably, the enhancement of mixing

754 strength by increased wind speed remains in the modified model and might be
755 amplified as the eddy diffusivity is increased. However, extremes in eddy diffusivity
756 was constrained with a fixed value; thus, it is reasonable to speculate that the
757 influence of high wind speed on the formation of lake thermal stratification was
758 limited. Moreover, our sensitivity analysis using offline WRF-Lake model (see
759 Supporting information 1) suggested that the effect of strong winds is most distinct
760 during autumn, in which the water temperature above 30 m increased, possibly due to
761 deeper mixed layer depth and larger amounts of water participated in the lake-air heat
762 exchange. The enhanced solar radiation increased the water temperature above 20 m
763 (Figure S2), which might increase the strength of lake stratification.

764 The changes in lake surface temperature may also influence the condition of the
765 overlying atmosphere. Generally, lakes could mitigate the regional climate by
766 decreasing the annual range of air temperature and increasing nearby precipitations
767 (Dai et al., 2018b; Wen et al., 2014). Therefore, we compared the temporal variations
768 of simulated near-surface air temperature and daily precipitation in the CTL and MOD
769 experiment as shown in Figure S9. It can be noted first that the MOD experiment has
770 similar seasonal patterns to that of CTL. The warmer lake surface in the MOD
771 experiment heated the overlying atmosphere. This alleviated the underestimation of
772 summer air temperature in CTL but also amplified the overestimation of winter air
773 temperature. The occurrences of rainfall events are consistent in these two
774 experiments. Simulated precipitation in spring is underestimated in both experiments.

The most distinct difference existed in May and June, in which the magnitude of precipitation in MOD was even less. This suggests that the volume of Lake Qiandaohu is not large enough to impact atmospheric circulations. Therefore, the improved lake scheme may slightly influence the magnitude of atmospheric variables but cannot change its overall pattern. The effects could be either improvement or deterioration, depending on the original biases of WRF.

4.2. Parameter sensitivity

4.2.1. Time-dependent light extinction coefficient

It has been described that darker surface waters tend to form shallower mixed layers owing to the less deeply penetrated radiation. This results in more turbulent heat loss at the lake surface and larger variation in the epilimnion temperature (Heiskanen et al., 2015; Zolfaghari et al., 2017). The results from Guseva et al. (2020) suggested that different 1D lake models respond similarly to changes in water clarity and that the thermocline depth increases in clear waters. However, the simulation results showed a slight increase in the thermocline depth when larger light extinction coefficients were used, which is indicated by the reduced negative biases in KD compared with those in CTL (Figure 10a). Although the direct influence of penetrated radiation is restricted in shallow layers, it seems that this heating effect has extended down to approximately 15 m since June (Figure 7a). This could possibly contribute to a deepening of the thermocline. The results also showed that a larger light extinction

coefficient generated a thicker metalimnion, which corresponds to the linear relationship deduced from in situ water temperature measurements in Lake Qiandaohu, where a negative correlation between metalimnion thickness and water transparency was found (Zhang et al., 2014). Therefore, it can be tentatively concluded that the response of lake stratification to changes in water clarity may differ in lakes with different depths and thermal regimes. It is difficult to determine the influence of light attenuation on lake stratification because research on this parameter at regional or global scales is still lacking. This literature deficiency may be attributed to insufficient high-frequency measurements of water clarity and water temperature. Satellite-derived series of water transparency combined with lake models may shed more light on this issue.

4.2.2. Initial lake water temperature in monomictic lakes

Sensitivity experiment of the calibrated initial lake temperature profile showed that this modification is crucial for generating realistic hypolimnion temperatures even though the influence of changes in the initial lake temperature profile on LSWT did not last for more than one month. This is unsurprising given that LSWT is driven by the surface energy balance, and its variation can be captured by lake models even in the absence of a reasonable subsurface temperature (Stepanenko et al., 2013). Monomictic lakes do not experience complete overturn in winter and thus cannot reset the deep water temperature like dicmictic lakes. Therefore, the underestimation of the hypolimnion temperature in monomictic lakes induced by initial conditions implies

insufficient heat storage and could eventually lead to shifts in thermal dynamic processes during long-term simulations (Perroud et al., 2009).

4.2.3. Simulating heat transfer in 1D lake models

The eddy diffusivity parameterization based on Henderson-Sellers (1985) struggles to simulate the mixing strength in deep lakes (Perroud et al., 2009; Stepanenko et al., 2010; Thiery et al., 2014b). Despite that, this type of model has been used widely in lake simulations because of its flexibility, which allows it to produce acceptable results without considerable modification (Martynov et al., 2010). Our results confirmed that the tuned model can simulate seasonal variation of the lake thermal structure with reasonable error during summer, suggesting that this model can be further applied to simulations in which the interannual variations of the lake thermal regime matter. It is believed that the 1D mixing processes can be theoretically tuned to imitate the behavior of that in a real lake based on available empirical formulas. But the limitation of original eddy diffusivity could not be completely solved by enlarging or shrinking it, which is a common approach (Bennington et al., 2014; Wu et al., 2020; Xiao et al., 2016). The results suggest that tuning eddy diffusivity affects only the thermal structure in the epilimnion and upper metalimnion as this coefficient decreases exponentially with depth and levels off below the thermocline with a magnitude far less than the molecular diffusivity. This implies little or no turbulence in the modeled deep layer, which is not the case in reality.

The vertical structure of the Henderson-Sellers eddy diffusivity raises two

838 questions. First, the heat diffusion between the thermocline and hypolimnion is
839 lacking in the modeled lake; therefore, the water temperature in the lower
840 metalimnion could not be well reproduced. It is apparent that the k_{eobs} concaved at
841 depths with large gradients and decreased mildly with increasing depth; in contrast,
842 the k_{esim} dropped sharply and became less than the molecular diffusivity between 15–
843 40 m. Thus, although Lake Qiandaohu formed two zones with steep temperature
844 gradients, it is believed that this conclusion is tenable in other deep lakes. Moreover,
845 ALBM and MTCR-1, which both uses Henderson-Sellers diffusivity, also failed to
846 reproduce the temporal and depth variability of vertical eddy diffusivity in a
847 temperate dimictic lake (Guseva et al., 2020), although the models generated
848 satisfactory thermal structure. Therefore, it is reasonable to infer that this issue not
849 only existed in WRF-Lake, but also in all advective-diffusive models based on the
850 same parameterization method.

851 The next problem is unresolved heat diffusion in the hypolimnion, for example,
852 internal seiches generated from hypolimnetic currents, that transfer wind energy from
853 the lake surface to turbulence at the bottom (Imberger, 1998). This deficiency exists in
854 selected 1D lake models that do not consider internal waves; even the more
855 sophisticated k-ε model can only calculate the turbulence above the thermocline
856 (Perroud et al., 2009), and thus the extra parameterization for turbulences in deep
857 layers is required. It has been found that the vertical diffusivity of heat in stratified
858 layers of many lakes can be described as $k = b(N^2)^m$, where m and b are constants

related to lake properties (Jassby and Powell, 1975). Therefore, some models such as the PROBE model (Svensson, 1978), the lake component in CLM 4.5, and an offline version of the WRF-Lake model (Wang et al., 2019) adopted this expression to mimic the unresolved mixing process in factual lakes. It is noteworthy that the weight of this additional term must be cautiously selected for a specific lake. Throughout the testing process, this added term was required for certain depths to better simulate the deepening of the metalimnion in the spring and early summer. However, during the decay of summer stratification, this term must be turned off or decreased to prevent over-mixing in the water column. Zhang et al. (2019) also found that the lake module in CLM 4.5 failed to reproduce the transition between stratification and overturn because of this arbitrary attached term, although it still worked well for some lakes (Wang et al., 2019). Overall, it seems that the inclusion of an enhanced term, such as that of other water mixing schemes and parameterization methods for major types of unresolved heat diffusion, is a compromise between computational cost and more complicated three-dimensional hydrodynamic models.

5. Conclusions

In the current study, the WRF-Lake model was improved to simulate the lake thermal regime over a monomictic deep Lake Qiandaohu by tuning four key model parameters, i.e., the initial lake water temperature profiles, light extinction coefficients, eddy diffusion coefficients, and the surface roughness lengths. We found that:

(1) The modified 1D lake model, WRF-Lake, simulated thermal structure of Lake Qiandaohu with satisfactory performance. The MBE and RMSE of LSWT between simulation results and in situ observations were reduced from –1.3 ℃ to –0.1 ℃ and 2.9 ℃ to 1.6 ℃, respectively. The evolution of lake stratification was well captured, which is indicated by three metrics. For example, the MBE of the thermocline depth decreased from 13.0 m to –1.7 m.

(2) The WRF model overpredicted the near-surface wind speed and downward shortwave radiation on the ground by an MBE of 2.7 m s^{-1} and 82.0 W m^{-2}, respectively. The impacts of high wind speed on simulating LSWT are in contrast to those of enhanced shortwave radiation but cannot be completely offset. The tuned maximum value of eddy diffusivity limited the effects of wind speed on mixing strength in the subsurface water layers.

(3) The initial lake water temperature determined the magnitude of the water temperature in the hypolimnion, which seldom experiences the water–air heat exchange caused by in complete mixing events in deep lakes. The light extinction coefficients and surface roughness lengths have the greatest impact on LSWT by governing the penetration of shortwave radiation in water layers and the exchange efficiency of heat and water vapor at the lake surface. However, they still slightly improve the model performance in simulating subsurface water temperature. Modifications of the eddy diffusivity improved the model performance in simulating the strength of

stratification.

(4) The Schmidt stability of Lake Qiandaohu varied with LSWT and was well simulated by the modified WRF-Lake model. Development of the thermocline from June to October is difficult to reproduce. The modified WRF-Lake reduced the annual MBE of the thermocline depth from –5.8 m to 1.0 m. The temporal variation of lake number and Wedderburn number derived from the simulation results agreed with those of the observations, although the magnitude showed negative biases. The large values of Schmidt stability and low values of lake number and Wedderburn number demonstrate that Lake Qiandaohu was strongly thermally stratified throughout the year, and the wind-driven internal waves in deep water and mixing were weak.

Thus, our results demonstrated that the modified WRF-Lake model could simulate LSWT and evolution of lake stratification with the lowest MBE and RMSE, which contributes to improvements in simulating lake thermal dynamics. Although geomorphology and optical characteristics differ between lakes, the revised version of WRF-Lake can be generalized to other study sites after minor modifications. Finally, more lake water temperature measurements are required to improve the representativeness of the mixing process parameterization scheme and enhance overall model performance.

Acknowledgments

This work was supported by the National Natural Science Foundation of China (Grant Nos. 41922005 and 41930760) and NIGLAS foundation (E1SL002). The computing resources granted by the Supercomputing Center of Lanzhou University are appreciated.

References

Anderson, E.J. et al., 2021. Seasonal overturn and stratification changes drive deep-water warming in one of Earth's largest lakes. Nature Communications, 12(1): 1688. DOI:10.1038/s41467-021-21971-1

Avolio, E. et al., 2017. Sensitivity analysis of WRF model PBL schemes in simulating boundary-layer variables in southern Italy: An experimental campaign. Atmospheric Research, 192: 58-71. DOI:10.1016/j.atmosres.2017.04.003

Balsamo, G. et al., 2012. On the contribution of lakes in predicting near-surface temperature in a global weather forecasting model. Tellus A: Dynamic Meteorology and Oceanography, 64(1). DOI:10.3402/tellusa.v64i0.15829

Bennington, V., Notaro, M., Holman, K.D., 2014. Improving climate sensitivity of deep lakes within a regional climate model and its impact on simulated climate. Journal of Climate, 27(8): 2886-2911. DOI:10.1175/JCLI-D-13-00110.1

Bruce, L.C. et al., 2018. A multi-lake comparative analysis of the General Lake Model (GLM): Stress-testing across a global observatory network. Environmental Modelling & Software, 102: 274-291. DOI:10.1016/j.envsoft.2017.11.016

Chen, F., Dudhia, J., 2001. Coupling an advanced land surface-hydrology model with the Penn State-NCAR MM5 modeling system. Part I: Model implementation and sensitivity. Monthly Weather Review, 129(4): 569-585. DOI:10.1175/1520-0493(2001)129<0569:Caalsh>2.0.Co;2

Chen, F. et al., 2011. The integrated WRF/urban modelling system: development, evaluation, and applications to urban environmental problems. International Journal of Climatology, 31(2): 273-288. DOI:10.1002/joc.2158

Dai, Y. et al., 2018a. The lake scheme of the Common Land Model and its performance evaluation. Chinese Science Bulletin, 63(28-29): 3002-3021. DOI:10.1360/n972018-00609

Dai, Y., Yao, T., Li, X., Ping, F., 2018b. The impact of lake effects on the temporal and spatial distribution of precipitation in the Nam Co basin, Tibetan Plateau. Quaternary International, 475: 63-69. DOI:10.1016/j.quaint.2016.01.075

Donis, D. et al., 2021. Stratification strength and light climate explain variation in chlorophyll *a* at the continental scale in a European multilake survey in a

heatwave summer. Limnology and Oceanography, 66(12): 4314-4333. DOI:10.1002/lno.11963
Edinger, J., Duttweiler, D., Geyer, J., 1968. The response of water temperature to meteorological conditions. Water Resources Research, 4. DOI:10.1029/WR004i005p01137
Gu, H., Jin, J., Wu, Y., Ek, M.B., Subin, Z.M., 2015. Calibration and validation of lake surface temperature simulations with the coupled WRF-lake model. Climatic Change, 129(3): 471-483. DOI:10.1007/s10584-013-0978-y
Gu, H., Ma, Z., Li, M., 2016. Effect of a large and very shallow lake on local summer precipitation over the Lake Taihu basin in China. Journal of Geophysical Research: Atmospheres, 121(15): 8832-8848. DOI:10.1002/2015jd024098
Guo, M. et al., 2021. Validation and sensitivity analysis of a 1‐D lake model across global lakes. Journal of Geophysical Research: Atmospheres, 126(4). DOI:10.1029/2020jd033417
Guseva, S. et al., 2020. Multimodel simulation of vertical gas transfer in a temperate lake. Hydrology and Earth System Sciences, 24(2): 697-715. DOI:10.5194/hess-24-697-2020
He, J. et al., 2020. The first high-resolution meteorological forcing dataset for land process studies over China. Scientific Data, 7(1): 1-11.
Heiskanen, J.J. et al., 2015. Effects of water clarity on lake stratification and lake‐atmosphere heat exchange. Journal of Geophysical Research: Atmospheres, 120(15): 7412-7428. DOI:10.1002/2014jd022938
Henderson-Sellers, B., 1985. New formulation of eddy diffusion thermocline models. Applied Mathematical Modelling, 9(6): 441-446. DOI:10.1016/0307-904X(85)90110-6
Hersbach, H. et al., 2020. The ERA5 global reanalysis. Quarterly Journal of the Royal Meteorological Society, 146(730): 1999-2049. DOI:10.1002/qj.3803
Hong, S.-Y., Noh, Y., Dudhia, J., 2006. A new vertical diffusion package with an explicit treatment of entrainment processes. Monthly Weather Review, 134(9): 2318-2341. DOI:10.1175/mwr3199.1
Hostetler, S.W., Bartlein, P.J., 1990. Simulation of lake evaporation with application to modeling lake level variations of Harney‐Malheur Lake, Oregon. Water Resources Research, 26(10): 2603-2612.
Huang, A. et al., 2019. Evaluating and improving the performance of three 1-D lake models in a large deep lake of the central Tibetan Plateau. Journal of Geophysical Research: Atmospheres, 124(6): 3143-3167. DOI:10.1029/2018JD029610
Imberger, J., 1998. Flux paths in a stratified lake: A review. Physical processes in lakes and oceans, 54: 1-17.
Imberger, J., Patterson, J.C., 1989. Physical limnology. Advances in applied mechanics, 27: 303-475.
Janjic, Z.I., 1994. The step-mountain eta coordinate model: further developments of

the convection, viscous sublayer, and turbulence closure schemes. Monthly Weather Review, 122(5): 927-945. DOI:10.1175/1520-0493(1994)122<0927:TSMECM>2.0.CO;2

Jassby, A., Powell, T., 1975. Vertical patterns of eddy diffusion during stratification in Castle Lake, California 1. Limnology and oceanography, 20(4): 530-543.

Jiménez, P.A., Dudhia, J., 2012. Improving the representation of resolved and unresolved topographic effects on surface wind in the WRF model. Journal of Applied Meteorology and Climatology, 51(2): 300-316. DOI:10.1175/jamc-d-11-084.1

Jiménez, P.A. et al., 2012. A revised scheme for the WRF surface layer formulation. Monthly Weather Review, 140(3): 898-918. DOI:10.1175/mwr-d-11-00056.1

Jousse, A., Hall, A., Sun, F., Teixeira, J., 2016. Causes of WRF surface energy fluxes biases in a stratocumulus region. Climate Dynamics, 46(1): 571-584.

Kraemer, B.M. et al., 2015. Morphometry and average temperature affect lake stratification responses to climate change. Geophysical Research Letters, 42(12): 4981-4988. DOI:10.1002/2015GL064097

Kumar, P., Bhattacharya, B.K., Pal, P., 2015. Evaluation of weather research and forecasting model predictions using micrometeorological tower observations. Boundary-Layer Meteorology, 157(2): 293-308.

Li, Y.-H., 1973. Vertical eddy diffusion coefficient in Lake Zürich. Schweizerische Zeitschrift für Hydrologie, 35(1): 1-7.

Lim, J.-O.J., Hong, S.Y., 2006. The WRF Single-Moment 6-Class Microphysics Scheme (WSM6). Asia-Pacific Journal of Atmospheric Sciences, 42(2): 129-151.

Liu, M. et al., 2019. Thermal stratification dynamics in a large and deep subtropical reservoir revealed by high-frequency buoy data. Sci. Total Environ., 651(Pt 1): 614-624. DOI:10.1016/j.scitotenv.2018.09.215

MacIntyre, S., Flynn, K.M., Jellison, R., Romero, J.R., 1999. Boundary mixing and nutrient fluxes in Mono Lake, California. Limnology and Oceanography, 44(3): 512-529.

Martynov, A., Sushama, L., Laprise, R., 2010. Simulation of temperate freezing lakes by one-dimensional lake models: performance assessment for interactive coupling with regional climate models. Boreal Environment Research, 15: 143-164.

Mironov, D.V., 2008. Parameterization of lakes in numerical weather prediction: Description of a lake model, DWD.

Oleson, K. et al., 2004. Technical description of the Community Land Model (CLM).

Oleson, K.W. et al., 2013. Technical description of version 4.5 of the Community Land Model (CLM) (No. NCAR/TN-503+STR). DOI:doi:10.5065/D6RR1W7M

Pan, X., Li, X., 2011. Validation of WRF model on simulating forcing data for Heihe River Basin. Sciences in Cold and Arid Regions, 3(4): 344-357.

Perroud, M., Goyette, S., Martynov, A., Beniston, M., Annevillec, O., 2009. Simulation of multiannual thermal profiles in deep Lake Geneva: A comparison of one-dimensional lake models. Limnology and Oceanography, 54(5): 1574-1594. DOI:10.4319/lo.2009.54.5.1574

Piccolroaz, S., Woolway, R.I., Merchant, C.J., 2020. Global reconstruction of twentieth century lake surface water temperature reveals different warming trends depending on the climatic zone (vol 35, pg 817, 2020). Climatic Change, 160(3): 443-443. DOI:10.1007/s10584-020-02720-7

Powell, T., Jassby, A., 1974. The estimation of vertical eddy diffusivities below the thermocline in lakes. Water Resources Research, 10(2): 191-198.

Qi, W., Liu, J., Yang, H., Chen, D., Feng, L., 2022. Assessments and Corrections of GLDAS2.0 Forcing Data in Four Large Transboundary Rivers in the Tibetan Plateau and Northeast China. Earth and Space Science, 9(1): e2020EA001576. DOI:10.1029/2020EA001576

Read, J.S. et al., 2011. Derivation of lake mixing and stratification indices from high-resolution lake buoy data. Environmental Modelling & Software, 26(11): 1325-1336. DOI:10.1016/j.envsoft.2011.05.006

Read, J.S., Rose, K.C., 2013. Physical responses of small temperate lakes to variation in dissolved organic carbon concentrations. Limnology and Oceanography, 58(3): 921-931.

Richardson, D.C. et al., 2017. Transparency, geomorphology and mixing regime explain variability in trends in lake temperature and stratification across Northeastern North America (1975–2014). Water, 9(6): 442.

Rose, K.C., Winslow, L.A., Read, J.S., Hansen, G.J.A., 2016. Climate-induced warming of lakes can be either amplified or suppressed by trends in water clarity. Limnology and Oceanography Letters, 1(1): 44-53. DOI:10.1002/lol2.10027

Ruiz-Arias, J.A., Arbizu-Barrena, C., Santos-Alamillos, F.J., Tovar-Pescador, J., Pozo-Vázquez, D., 2016. Assessing the surface solar radiation budget in the WRF Model: A spatiotemporal analysis of the bias and its causes. Monthly Weather Review, 144(2): 703-711. DOI:10.1175/mwr-d-15-0262.1

Schmid, M., Hunziker, S., Wüest, A., 2014. Lake surface temperatures in a changing climate: a global sensitivity analysis. Climatic Change, 124(1-2): 301-315. DOI:10.1007/s10584-014-1087-2

Schmid, M., Read, J., 2021. Heat Budget of Lakes, Reference Module in Earth Systems and Environmental Sciences. Elsevier. DOI:10.1016/B978-0-12-819166-8.00011-6

Schmidt, W., 1928. Über Die Temperatur-Und Stabili-Tätsverhältnisse Von Seen. Geografiska Annaler, 10(1-2): 145-177.

Shatwell, T., Adrian, R., Kirillin, G., 2016. Planktonic events may cause polymictic-dimictic regime shifts in temperate lakes. Sci Rep, 6: 24361. DOI:10.1038/srep24361

Shi, Y. et al. (2022). Drivers of warming in Lake Nam Co on Tibetan Plateau over the past 40 years. Journal of Geophysical Research: Atmospheres, 127, e2021JD036320. DOI: 10.1029/2021JD036320

Skamarock, W.C. et al., 2019. A description of the advanced research WRF model version 4. National Center for Atmospheric Research: Boulder, CO, USA: 145.

Stauffer, D.R., Seaman, N.L., 1994. Multiscale four-dimensional data assimilation. Journal of Applied Meteorology, 33(3): 416-434. DOI:10.1175/1520-0450(1994)033<0416:Mfdda>2.0.Co;2

Stepanenko, V. et al., 2010. First steps of a lake model intercomparison project: LakeMIP. Boreal Environment Research, 15: 191-202.

Stepanenko, V. et al., 2014. Simulation of surface energy fluxes and stratification of a small boreal lake by a set of one-dimensional models. Tellus A: Dynamic Meteorology and Oceanography, 66(1): 21389. DOI:10.3402/tellusa.v66.21389

Stepanenko, V.M. et al., 2013. A one-dimensional model intercomparison study of thermal regime of a shallow, turbid midlatitude lake. Geoscientific Model Development, 6(4): 1337-1352. DOI:10.5194/gmd-6-1337-2013

Su, R. et al., 2022. Summer lake destratification phenomenon: A peculiar deep lake on the Tibetan Plateau. Frontiers in Earth Science, 10: 839151. DOI:10.3389/feart.2022.839151

Subin, Z.M., Riley, W.J., Mironov, D., 2012. An improved lake model for climate simulations: Model structure, evaluation, and sensitivity analyses in CESM1. Journal of Advances in Modeling Earth Systems, 4. DOI:10.1029/2011ms000072

Svensson, U., 1978. A mathematical model of the seasonal thermocline. Institutionen För Teknisk Vattenresurslära, Lunds Tekniska Högskola, Lunds ….

Thiery, W. et al., 2014a. Understanding the performance of the FLake model over two African Great Lakes. Geoscientific Model Development, 7(1): 317-337. DOI:10.5194/gmd-7-317-2014

Thiery, W.I.M. et al., 2014b. LakeMIP Kivu: evaluating the representation of a large, deep tropical lake by a set of one-dimensional lake models. Tellus A: Dynamic Meteorology and Oceanography, 66(1). DOI:10.3402/tellusa.v66.21390

Thompson, R., 1980. Response of a numerical model of a stratified lake to wind stress, Proc. Second Int. Symp. Stratified Flows, IAHR, 1980, pp. 562-570.

Till, A., Rypel, A.L., Bray, A., Fey, S.B., 2019. Fish die-offs are concurrent with thermal extremes in north temperate lakes. Nature Climate Change, 9(8): 637-641. DOI:10.1038/s41558-019-0520-y

Wang, F. et al., 2019. Evaluation of the WRF lake module (v1.0) and its improvements at a deep reservoir. Geoscientific Model Development, 12(5): 2119-2138. DOI:10.5194/gmd-12-2119-2019

Wen, L., Lyu, S., li, Z., Zhao, L., Nagabhatla, N., 2014. Impact of two biggest lakes on local temperature and precipitation in the Yellow River source region of the

Tibetan Plateau. Advances in Meteorology.
Wild, M., 2005. Solar radiation budgets in atmospheric model intercomparisons from a surface perspective. Geophysical Research Letters, 32(7).
Woolway, R.I., Jennings, E., Carrea, L., 2020. Impact of the 2018 European heatwave on lake surface water temperature. Inland Waters, 10(3): 322-332. DOI:10.1080/20442041.2020.1712180
Woolway, R.I. et al., 2019. Northern Hemisphere Atmospheric Stilling Accelerates Lake Thermal Responses to a Warming World. Geophysical Research Letters, 46(21): 11983-11992. DOI:10.1029/2019gl082752
Woolway, R.I. et al., 2021. Phenological shifts in lake stratification under climate change. Nature Communications, 12(1). DOI:10.1038/s41467-021-22657-4
Woolway, R.I. et al., 2018. Geographic and temporal variations in turbulent heat loss from lakes: A global analysis across 45 lakes. Limnology and Oceanography, 63(6): 2436-2449. DOI:10.1002/lno.10950
Wu, Y. et al., 2020. Improvements of the coupled WRF-Lake model over Lake Nam Co, Central Tibetan Plateau. Climate Dynamics, 55(9-10): 2703-2724. DOI:10.1007/s00382-020-05402-3
Xiao, C., Lofgren, B.M., Wang, J., Chu, P.Y., 2016. Improving the lake scheme within a coupled WRF‐lake model in the Laurentian Great Lakes. Journal of Advances in Modeling Earth Systems, 8(4): 1969-1985. DOI:10.1002/2016ms000717
Xu, L., Liu, H., Du, Q., Wang, L., 2016. Evaluation of the WRF-lake model over a highland freshwater lake in southwest China. Journal of Geophysical Research: Atmospheres, 121(23): 13,989-14,005. DOI:10.1002/2016jd025396
Yang, F. et al., 2017. Evaluation of multiple forcing data sets for precipitation and shortwave radiation over major land areas of China. Hydrology and Earth System Sciences, 21(11): 5805-5821. DOI:10.5194/hess-21-5805-2017
Yang, K., He, J., Tang, W., Qin, J., Cheng, C.C., 2010. On downward shortwave and longwave radiations over high altitude regions: Observation and modeling in the Tibetan Plateau. Agricultural and Forest Meteorology, 150(1): 38-46.
Zamani, B., Koch, M., Hodges, B.R., 2021. A potential tipping point in the thermal regime of a warm monomictic reservoir under climate change using three-dimensional hydrodynamic modeling. Inland Waters, 11(3): 315-334.
Zeng, X., Zhao, M., Dickinson, R.E., 1998. Intercomparison of bulk aerodynamic algorithms for the computation of sea surface fluxes using TOGA COARE and TAO data. Journal of Climate, 11(10): 2628-2644.
Zhang, Q. et al., 2019. Improving lake mixing process simulations in the Community Land Model by using K profile parameterization. Hydrology and Earth System Sciences, 23(12): 4969-4982. DOI:10.5194/hess-23-4969-2019
Zhang, Y. et al., 2014. Thermal structure and response to long-term climatic changes in Lake Qiandaohu, a deep subtropical reservoir in China. Limnology and Oceanography, 59(4): 1193-1202. DOI:10.4319/lo.2014.59.4.1193

Zolfaghari, K., Duguay, C.R., Kheyrollah Pour, H., 2017. Satellite-derived light extinction coefficient and its impact on thermal structure simulations in a 1-D lake model. Hydrology and Earth System Sciences, 21(1): 377-391. DOI:10.5194/hess-21-377-2017

Supplemental materials to "Numerical simulation of thermal stratification in Lake Qiandaohu using an improved WRF-Lake model "

Xiwen Wang[a,b], Weijia Wang[b,c], Yuan He[d], Shulei Zhang[e], Wei Huang[a], R. Iestyn Woolway[f], Kun Shi[b,c*], Xiaofan Yang[d*]

[a] Key Laboratory of Western China's Environmental Systems (Ministry of Education), College of Earth and Environmental Sciences, Lanzhou University, Lanzhou, 730000, China

[b] Taihu Laboratory for Lake Ecosystem Research, State Key Laboratory of Lake Science and Environment, Nanjing Institute of Geography and Limnology, Chinese Academy of Sciences, Nanjing 210008, China

[c] University of Chinese Academy of Sciences, Beijing 100049, China

[d] State Key Laboratory of Earth Surface Processes and Resource Ecology, Faculty of Geographical Science, Beijing Normal University, Beijing 100875, China

[e] School of Atmospheric Sciences, Sun Yat-sen University, Guangzhou, China

[f] School of Ocean Sciences, Bangor University, Menai Bridge, Anglesey, Wales

Corresponding author:

Kun Shi: kshi@niglas.ac.cn

Xiaofan Yang: xfyang@bnu.edu.cn

Contents

This supplementary material contains Supporting Information 1-2, Figure S1-16, and Table S1-3.

Supporting information 1: Sensitivity analysis of WRF-Lake in offline mode

To provide practical guidance for the possible consequences of inaccurate forcings, we performed a sensitivity analysis by running the default WRF-Lake offline. In this way the meteorological forcings will not be affected by the lake condition during simulations. The input forcings come from the ERA5 reanalysis with hourly temporal and 0.25° spatial resolution. Other settings (e.g., initial conditions) are the same as CTL. We conducted five sensitivity experiments (Table S1) and a control experiment (BASE). The mean bias errors against BASE are shown in Figure S2. It is clear that the influences of overestimated wind speed and shortwave radiation are mainly on the subsurface water layer at annual scale. High wind speed caused little cooling effect during summer and increased water temperature in shallow layers during the cool-down period in the autumn. Our results suggested lake surface water temperature (averaged over 0-2 m) could increase 0.22 °C if wind speed increases by 1.41 m s^{-1}, and increase 0.03 °C if shortwave radiation increases by 1 W m^{-2}. The latter is similar to the findings in Schmid et al. (2014). For the lake thermal structure, the overestimated shortwave radiation could result in warmer temperature above 20 m. Stronger wind largely increases the water temperature above 30 m in the autumn.

Table S1 Five experiments for sensitivity analysis.

Case	Description
BASE	Control experiment
T	Increase 2-m air temperature by 1 °C
Q	Increase 2-m specific humidity by 0.001 kg kg^{-1}
Wind	Increase both 10-m U and V components of wind by 1 m s^{-1}
SW	Increase downward shortwave radiation at the ground by 1 W m^{-2}
LW	Increase downward longwave radiation at the ground by 1 W m^{-2}

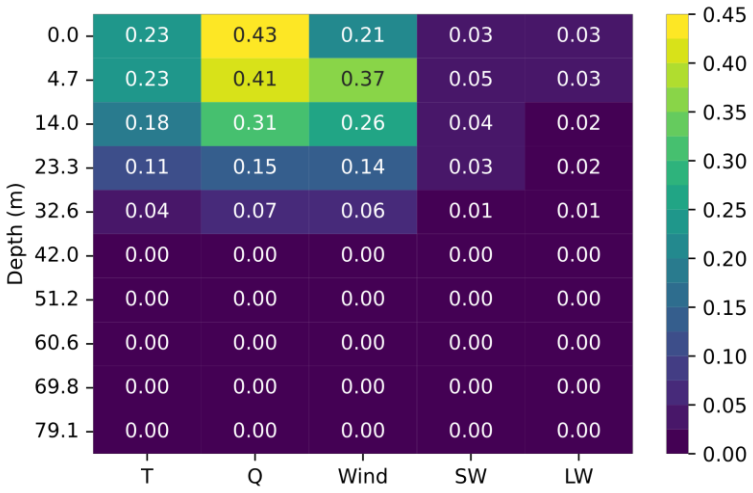

Figure S1 Mean bias error of lake water temperature between BASE and other experiments during 2016.

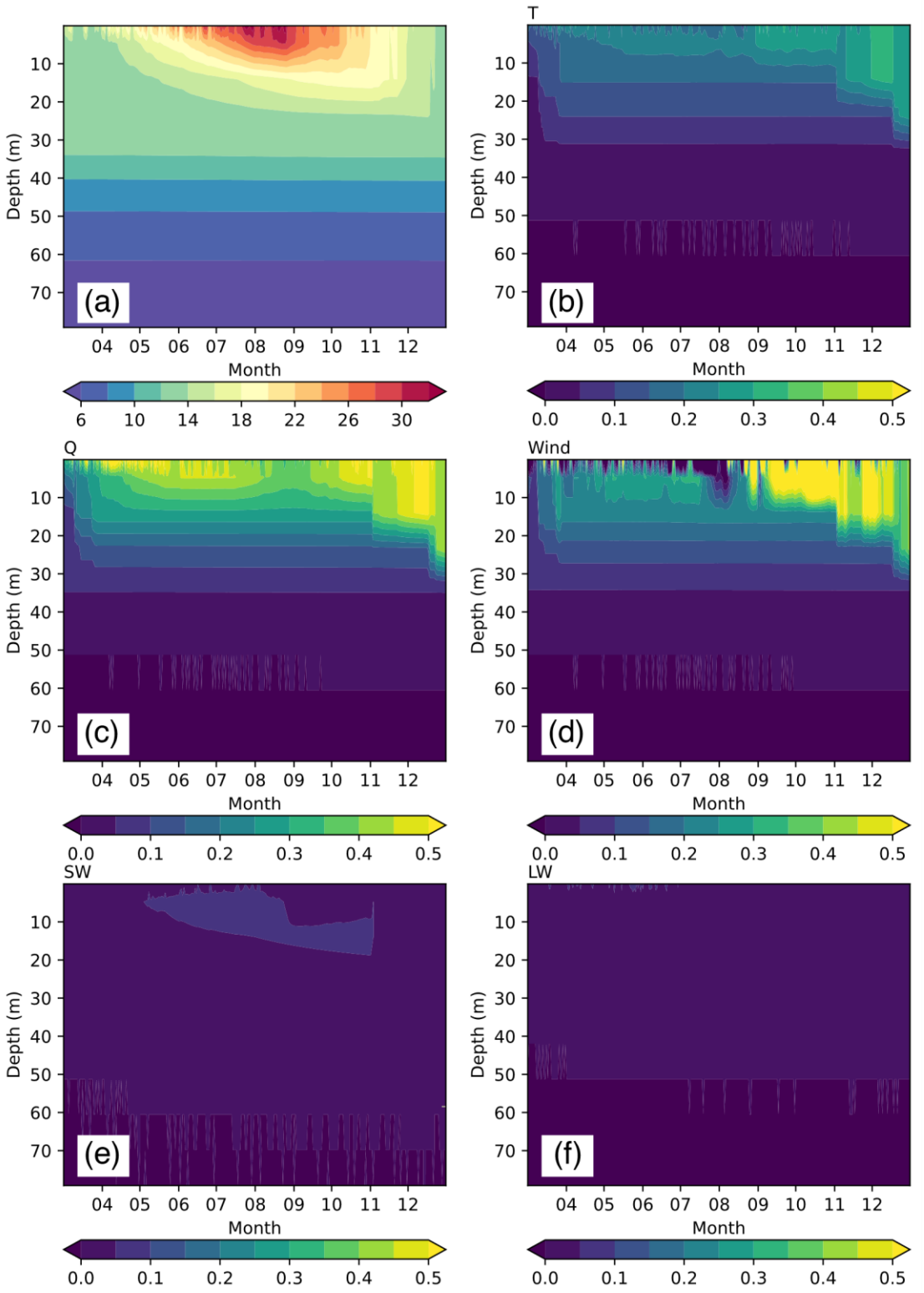

Figure S2 (a) Lake water temperature (°C) in the BASE experiment and the differences between BASE and (b) T, (c) Q, (d) Wind, (e) SW and (f) LW.

Supporting information 2: Using a 25-layer discretization method

We performed two additional numerical experiments using a 25-layer discretization method (Table S2) based on the CTL and MOD experiment respectively, denoted as CTL_25 and MOD_25 (Figure S3-4). The results showed that increasing vertical layers produces smoother water temperature profile during the development of thermal stratification. The mixing strength above 10 m was promoted, although the overall distribution of water temperature below 20 m was only sightly affected. The root mean square error (RMSE) for the surface water temperature (the average of 0-2 m) in MOD_25 is 1.18 °C, smaller than that of MOD (1.59 °C). However, the negative bias above 20 m and the positive bias below it got worse in MOD_25.

Table S2 The layer thickness and depth of each layer center at Daba buoy (~ 93 m) using 25-layer discretization method.

Layer	Thickness (m)	Depth (m)
1	0.1	0.05
2	0.465	0.3325
3	0.465	0.7975
4	0.465	1.2625
5	0.465	1.7275
6	0.93	2.425
7	0.93	3.355
8	0.93	4.285
9	0.93	5.215
10	1.395	6.3775
11	1.395	7.7725
12	1.395	9.1675
13	1.395	10.5625
14	3.72	13.12
15	3.72	16.84
16	4.65	21.025
17	4.65	25.675
18	6.51	31.255
19	6.51	37.765
20	6.51	44.275
21	6.51	50.785
22	9.7185	58.89925
23	9.7185	68.61775
24	9.7185	78.33625
25	9.7185	88.05475

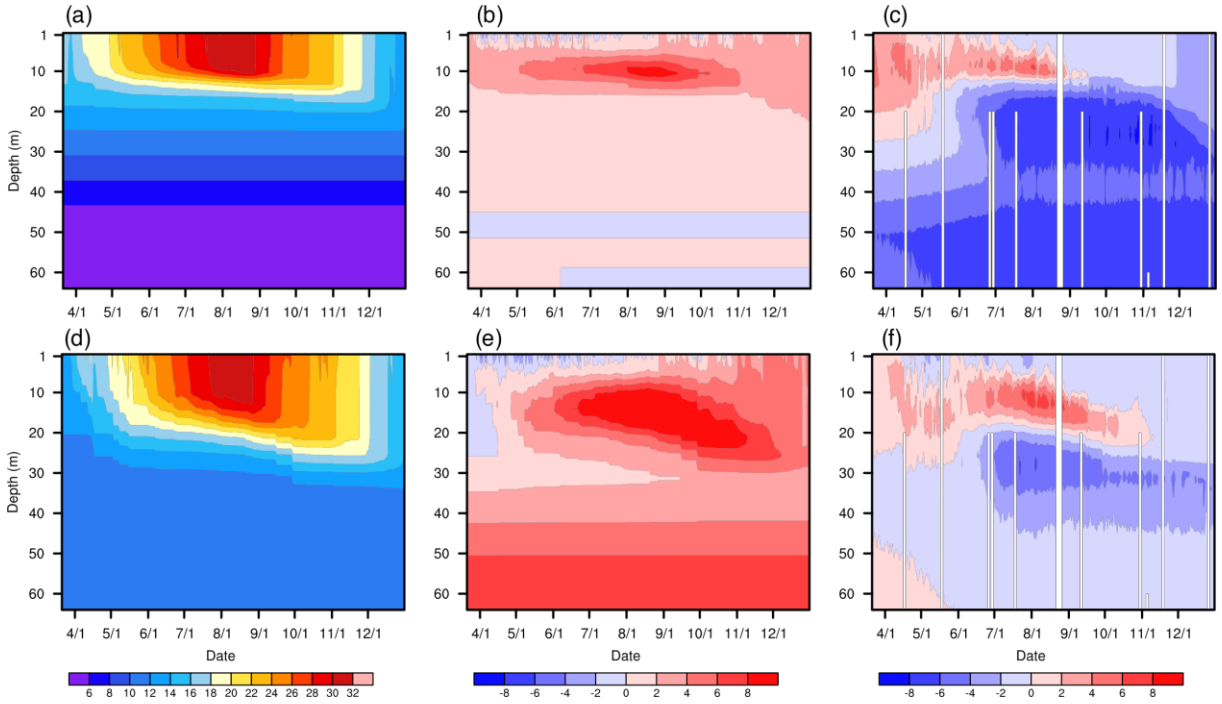

Figure S3 The lake water temperature (°C) at Daba simulated by (a) CTL_25 and (d) MOD_25 from 2016-03-21 to 2016-12-31. The differences between CTL and CTL_25 (b), the observations and CTL_25 (c), CTL and MOD_25 (e) and the observations and MOD_25 (f).

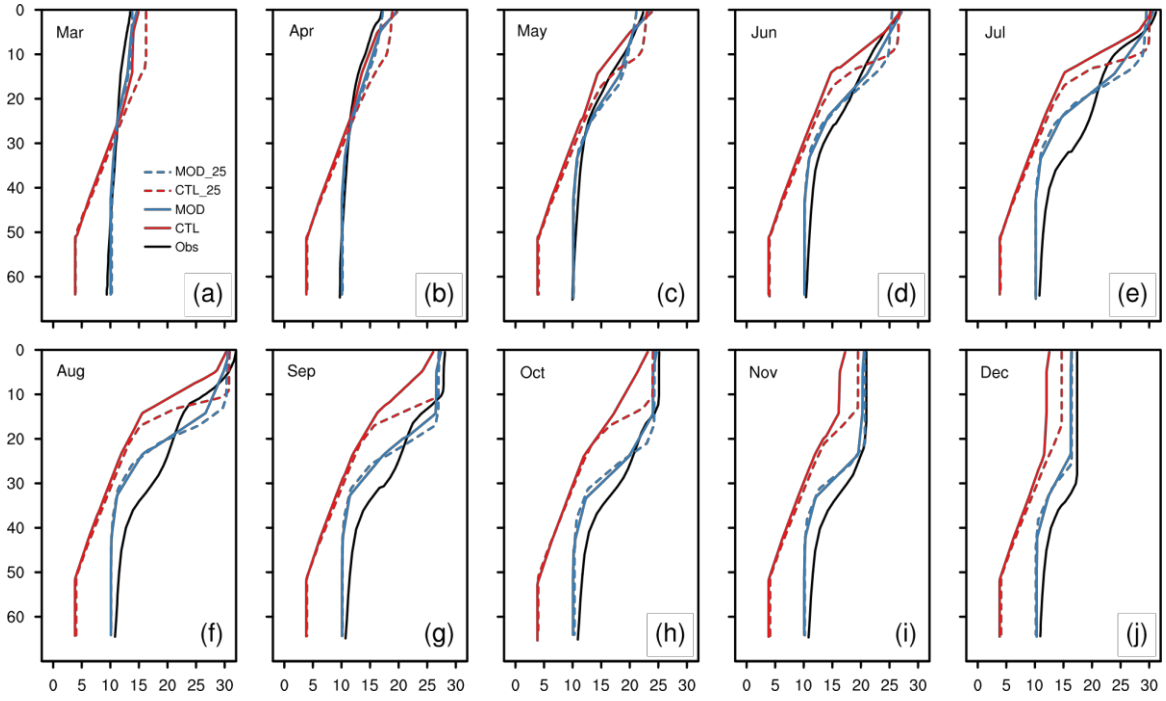

Figure S4 The monthly lake water temperature profile derived from the observations simulated by CTL, MOD, CTL_25 and MOD_25.

Figure S5 Light extinction coefficients in photosynthetically active radiation region (400–700 nm).

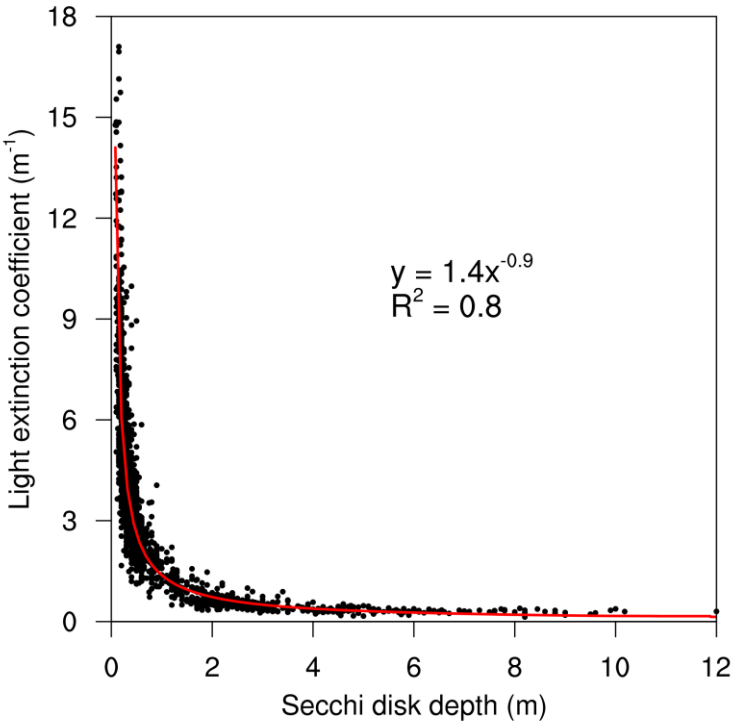

Figure S6 Daily variation of (a) lake surface water temperature (℃), (b) sensible heat flux (W m^{-2}), and (c) latent heat flux (W m^{-2}) differences between CTL and other sensitivity.

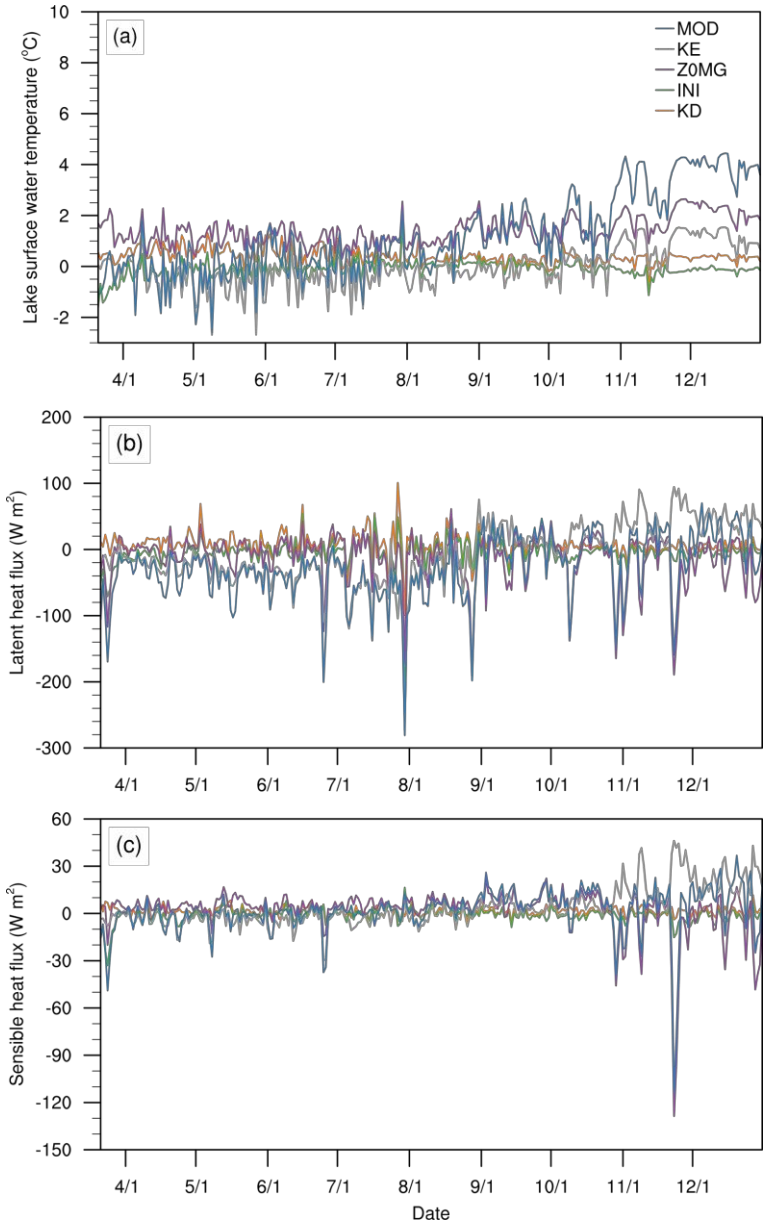

Figure S7 Monthly vertical profiles of the observed water temperature at the Daba station.

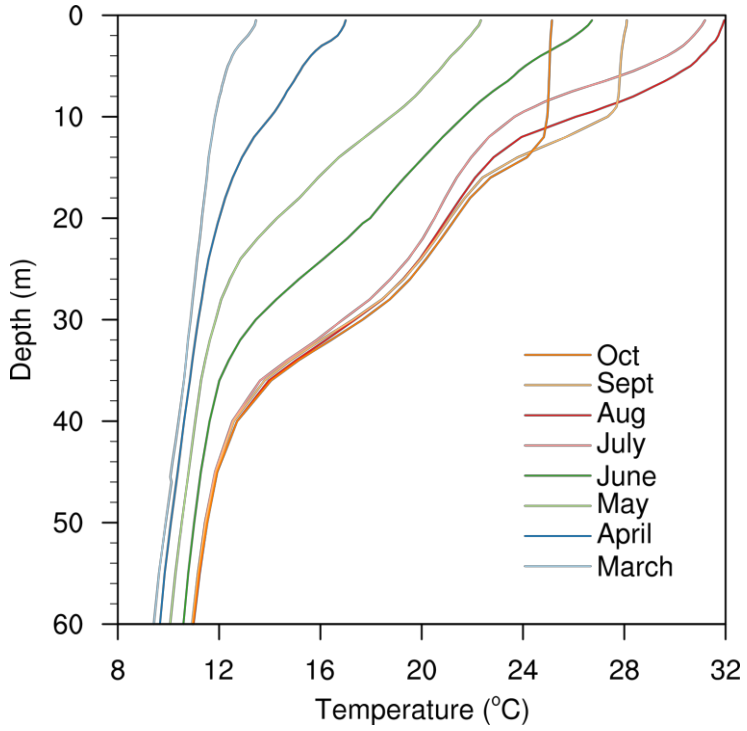

Figure S8 Daily 10-m wind speed (m s^{-1}) from the ERA5 reanalysis (red line) and observations at the Chun'an weather station (black line). Mean bias error (MBE) and root mean square error (RMSE) between them are –0.1 m s^{-1} and 0.9 m s^{-1}, respectively.

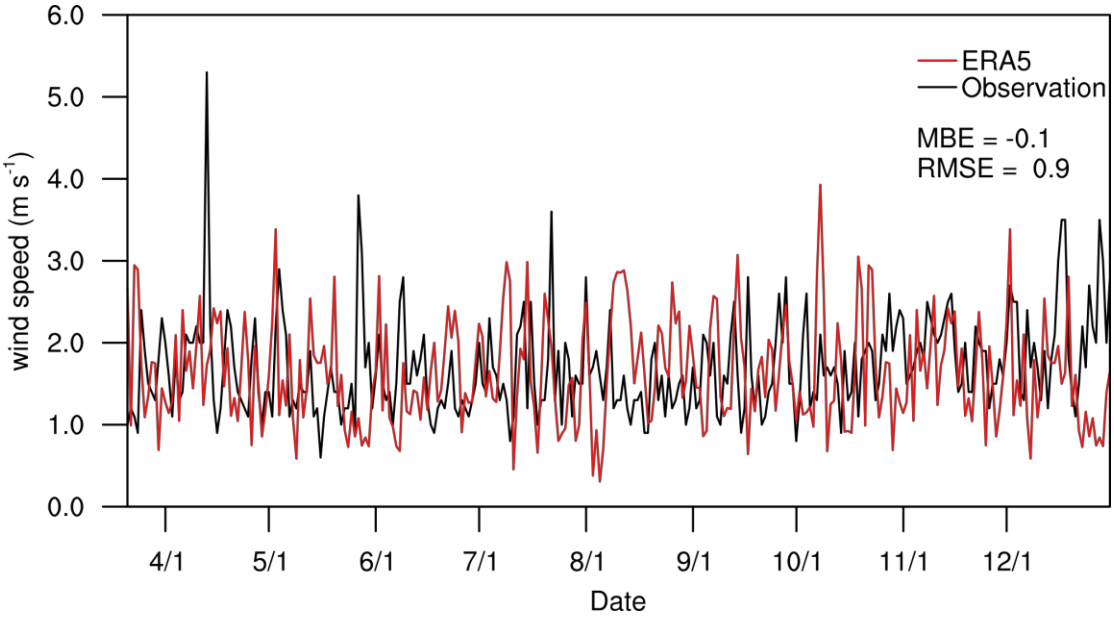

Figure S9 The 2-m air temperature (°C) and 24h rainfall (mm) observed by Chun'an weather station and simulated by CTL and MOD from March 21 2016 and December 31 2016.

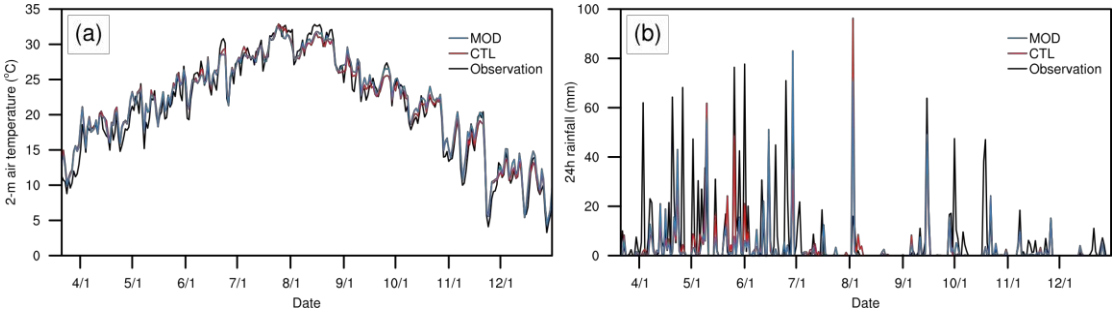

Figure S10 Differences between lake water temperature (°C) simulated by (a) CTL, (b) KD, (c) INI, (d) Z0MG, (e) KE, and (f) MOD.

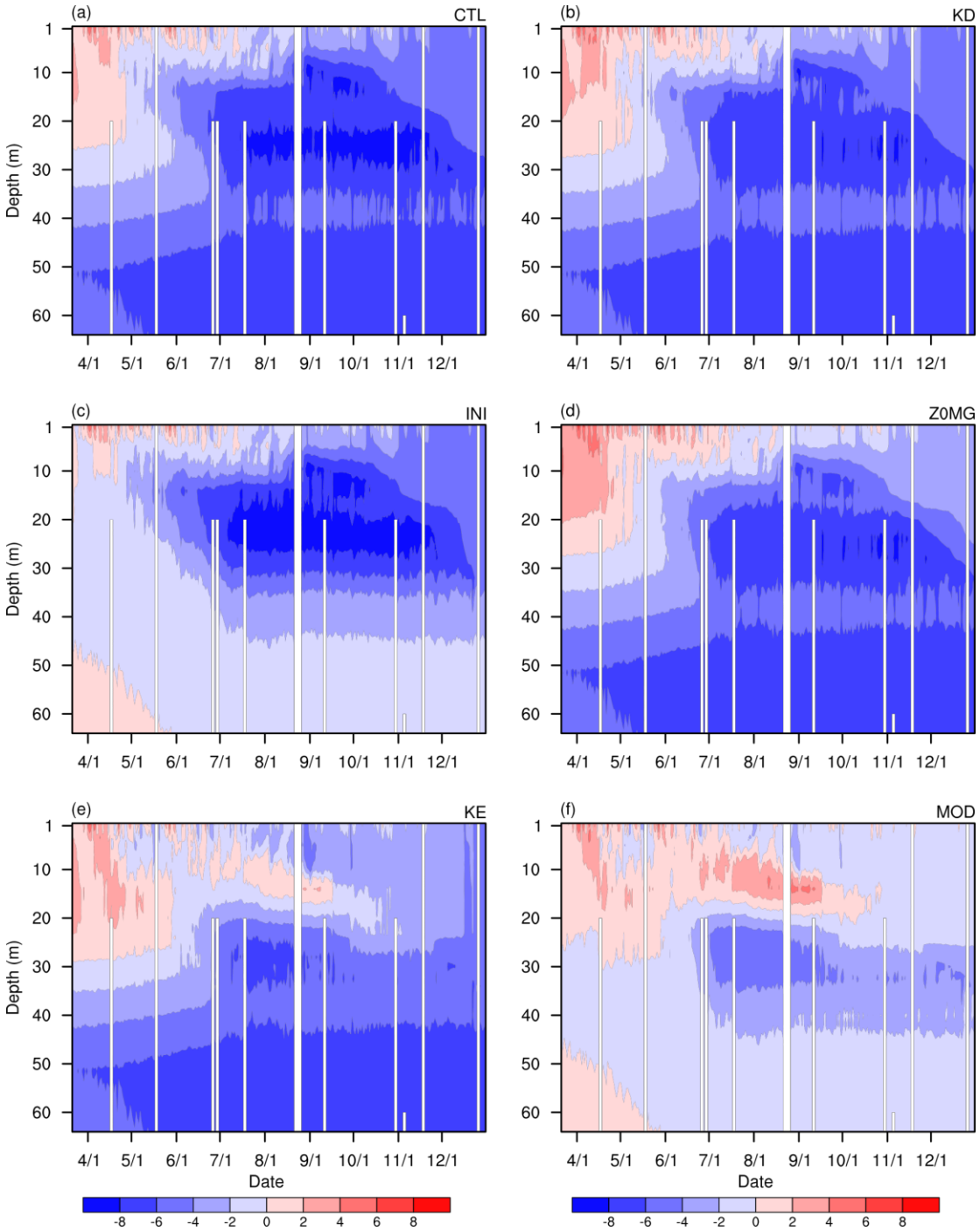

Figure S11 Monthly vertical temperature profiles for the first 65 m water in 2016.

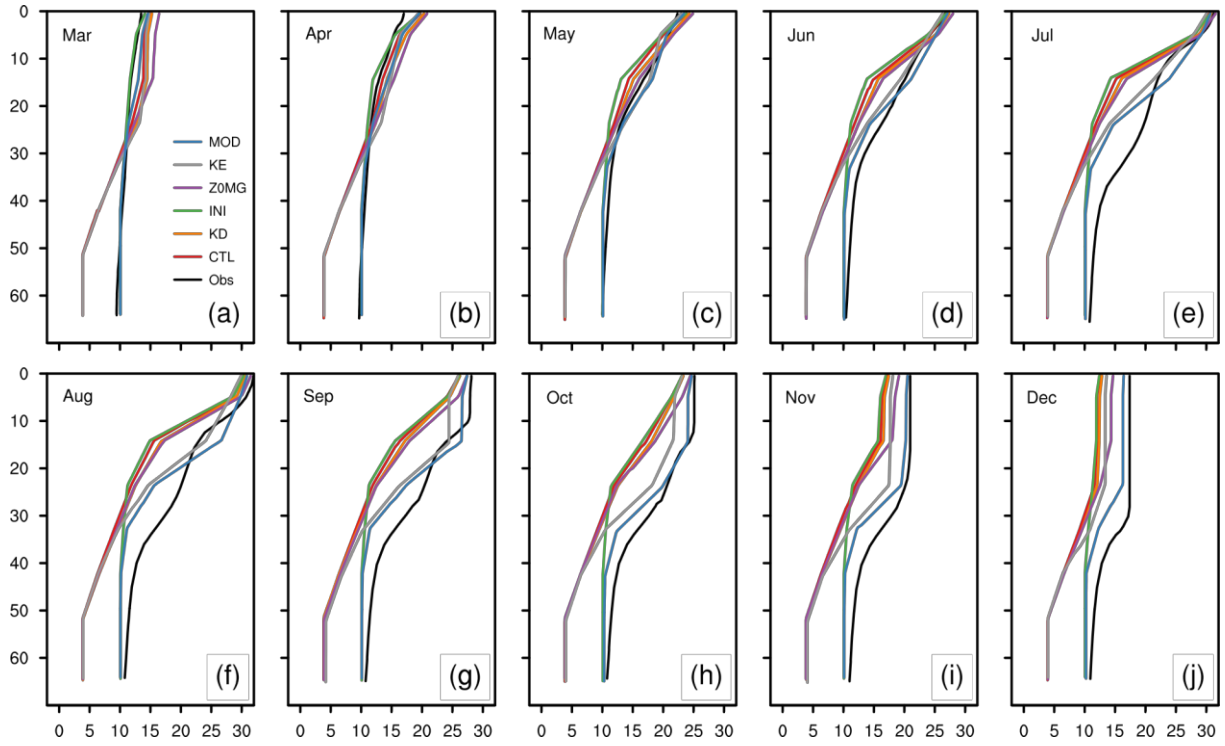

Figure S12 (a) Ri and (b) k_e (m^2 s^{-1}) at 04:00 UTC each day from 2016-03-21 to 2016-12-31. The blank at the bottom denotes missing values of the last vertical layer.

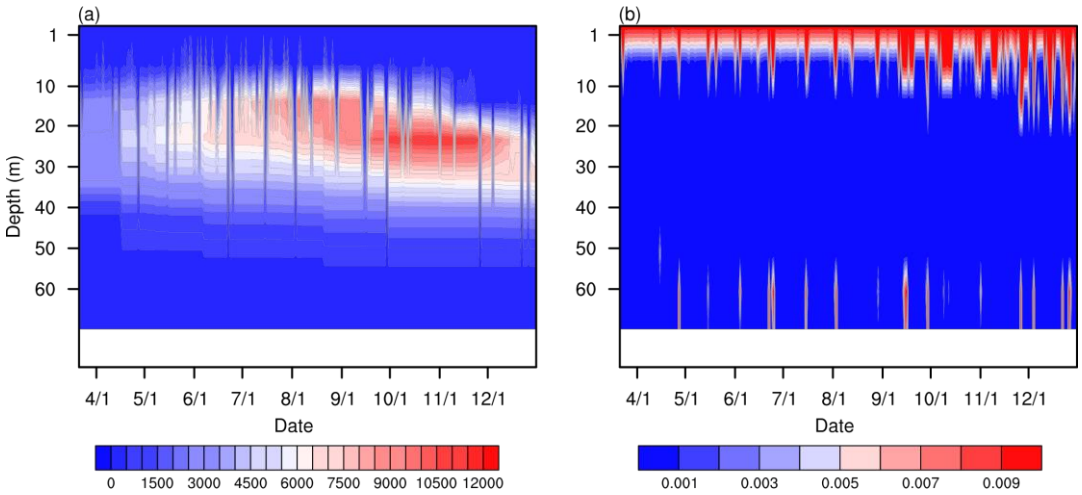

Figure S13 The time-averaged (a-b) 2-m air temperature (K), (c-d) 10-m wind speed (m s^{-1}), (e-f) surface downward shortwave radiation (W m^{-2}) and (g-h) surface longwave radiation (W m^{-2}) from 2016-03-21 to 2016-12-31. The first column shows the reanalysis and the second shows the simulation results. 2-m air temperature and 10-m wind speed are compared with ERA5. The shortwave and longwave radiation are compared with CMFD.

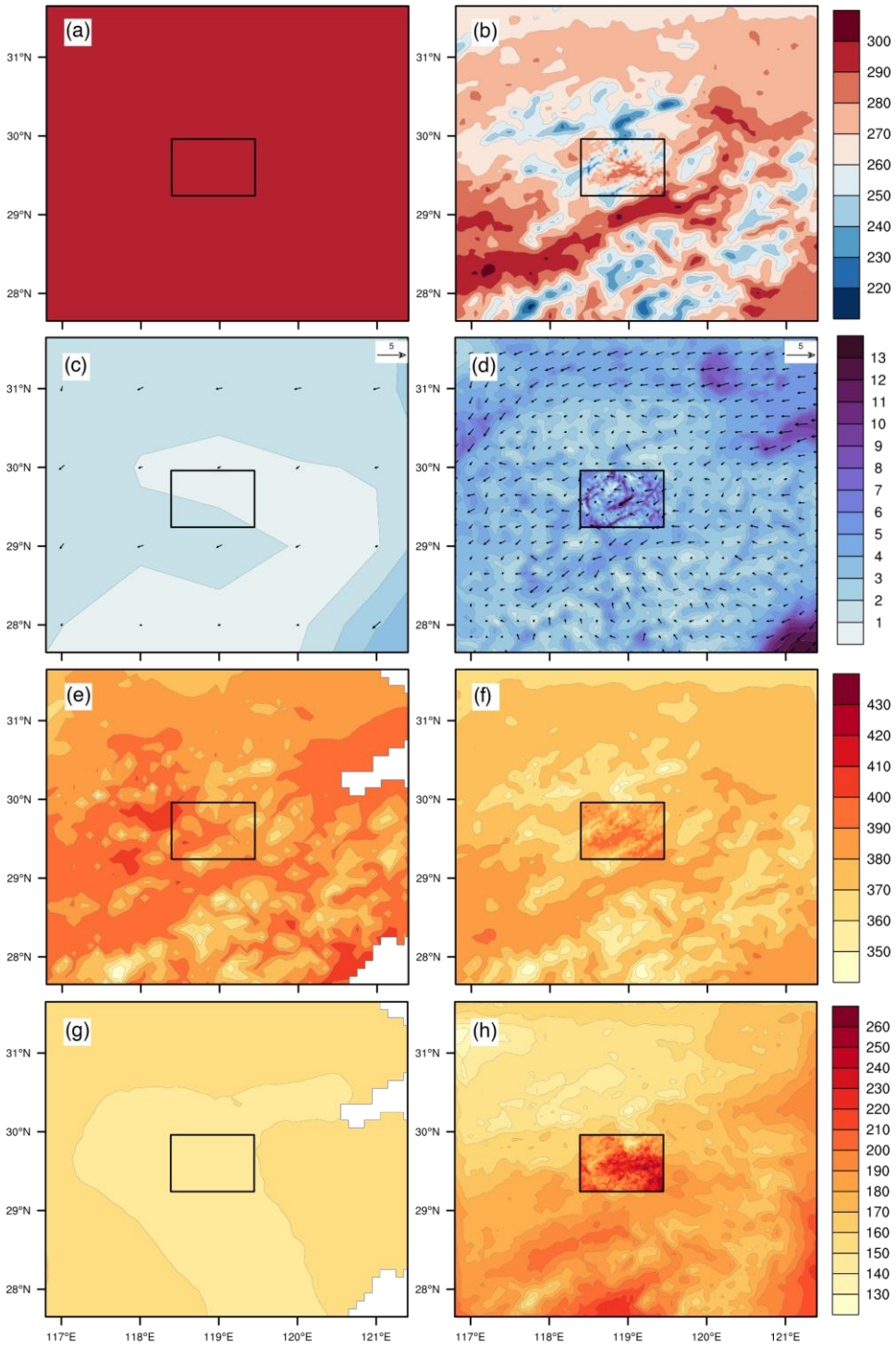

Figure S14 Same as Figure S13 but for the 2-m relative humidity (%), compared with ERA5.

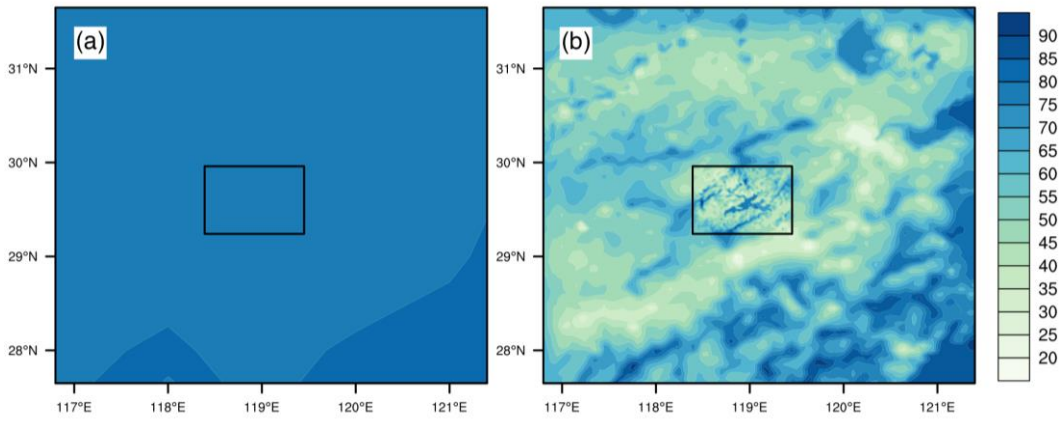

Figure S15 The lake water temperature of the top model layer (0.05 m) of CTL (a) and its difference against KD (b), INI (c), Z0MG (d), KE (e), and MOD (f).

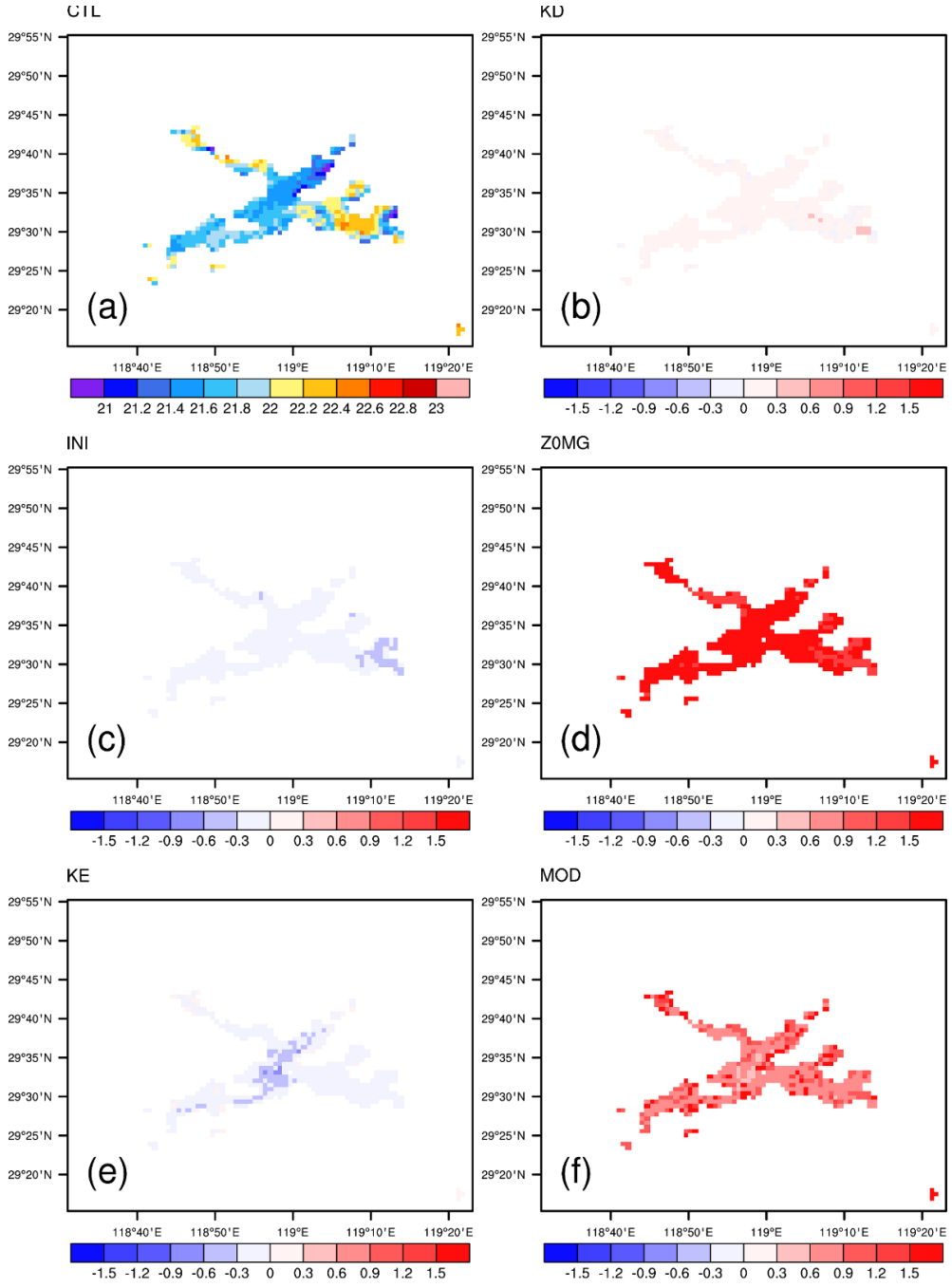

1288 Figure S16 The simulated lake water temperature (°C) and its differences with CTL.

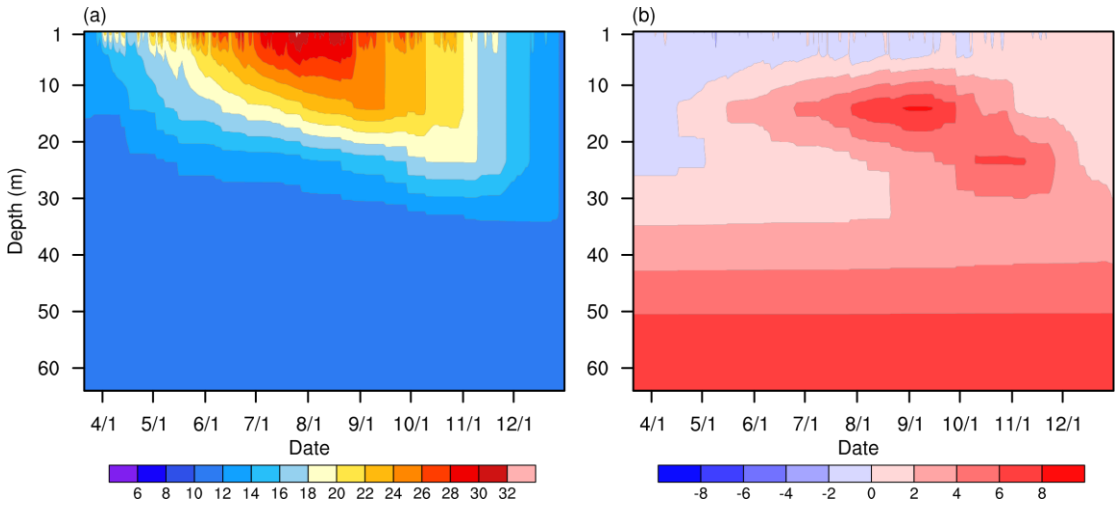

1289

Table S3 Mean bias error (MBE) and root mean square error (RMSE) of lake water temperature at different lake depth (0-2 m, 9-11 m, 19-21 m and 39-41 m), bottom depth of metalimnion (metaB), thickness of metalimnion (metaTh) and thermocline depth (thermD).

	Case	0-2 m	9-11 m	19-21 m	39-41 m	metaB	metaTh	thermD
MBE	CTL	-1.29	-3.59	-5.06	-5.02	12.96	-3.92	-5.8
	KD	-0.89	-2.85	-4.44	-4.83	-13.39	-5.01	-7.85
	INI	-1.38	-4.17	-5.75	-1.87	13.96	-3.28	-5.25
	Z0MG	0.1	-1.9	-4.08	-4.83	12.03	1.34	2.35
	KE	-1.31	-1.17	-1.71	-4.7	15.99	-3.97	-5.5
	KE_INI	-1.5	-1.78	-2.48	-1.65	-4.13	0.13	-0.82
	MOD	-0.08	0.46	-0.6	-1.62	-1.71	0.51	0.95
RMSE	CTL	2.87	4.54	6.04	5.33	18.88	7.51	12.1
	KD	2.76	3.99	5.49	5.14	16.33	8.81	13.12
	INI	2.87	4.85	6.57	2.15	18.51	6.69	11.1
	Z0MG	2.25	3.25	5.21	5.14	18.29	6	9.73
	KE	2.55	2.39	2.7	5	19.62	6.71	10.54
	KE_INI	2.58	2.47	3.01	1.88	9.21	5.01	9.02
	MOD	1.59	1.51	1.25	1.85	8.08	4.74	8.75